LEARN LOW-DIMENSIONAL SHORTEST PATH REPRESENTATION OF LARGE-SCALE AND COMPLEX GRAPHS

Anonymous authors
Paper under double-blind review

ABSTRACT

Estimation of Shortest-Path (SP) distance lies at the heart of network analysis tasks. Along with the rapid emergence of large-scale and complex graphs, approximate SP-representing algorithms that transform a graph into compact and low-dimensional representations are critical for fast and scalable online analysis. Among different approaches, learning-based representation methods have made a breakthrough both in response time and accuracy. Several competitive works in learning-based methods heuristically leverage truncated random walk and optimization of node-cooccurrence likelihood on the arbitrary linkage for SP representation learning. However, they have limitations on both exploration range and distance preservation. We propose in this paper an efficient and interpretable SP representation method called Betweenness Centrality-based Distance Resampling (BCDR). First, we prove that betweenness centrality-based random walk can occupy a wider exploration range of distance due to its awareness of high-order path structures. Second, we leverage distance resampling to simulate random shortest paths from original paths and prove that the optimization on such shortest paths preserves distance relations via implicitly decomposing SP distance-based similarity matrix. BCDR yields an average improvement of 30% accuracy and 25-30% query speed, compared to all existing approximate methods when evaluated on a broad class of real-world and synthetic graphs with diverse sizes and structures.

1 INTRODUCTION

Estimation of Shortest Path (SP) distance lies at the heart of many network analysis tasks, such as centrality computation (Schönfeld & Pfeffer, 2021), node separation (Houidi et al., 2020), community detection (Zhang et al., 2020; Asif et al., 2022), which contributes to enormous applications in social relationship analysis (Carlton, 2020; Melkonian et al., 2021; Chen et al., 2021; Zaki et al., 2021; Parveen & Varma, 2021), biomedical structure prediction (Yue et al., 2019; Galovičová et al., 2021; Sokolowski & Wasserman, 2021), learning theory (Yang et al., 2021; Yuan et al., 2021), optimization (Melkonian et al., 2021; Rahmad Syah et al., 2021; Jiang et al., 2021), etc. Nowadays, a key challenge of computing SP distance is the prohibitive complexity in very large and complex graphs. e.g., for a dense undirected graph with N nodes and k queries, the time complexity of A* (Hart et al., 1968) and Dijkstra algorithm (Thorup & Zwick, 2004) are up to $O(kN^2)$ and $O(kN \log N)$ for unweighted and weighted graph, respectively.

To address this issue, various kinds of methods (Cohen et al., 2003; Fu et al., 2013; Akiba et al., 2013; Delling et al., 2014; Farhan et al., 2019; Liu et al., 2021) have been designed to answer exact distance in microseconds online via indexing or compressing techniques, which suffer huge storage costs on all pair SP distance representations and fail to reflect latent sub-structures in graphs for scalable queries (see Figure 1). Highly concise SP representation for large-scale and complex graphs remains to be studied yet. Regarding this, a surging number of approximate SP-representing algorithms that transform a graph into compact and low-dimensional representations are thus critical for fast and scalable online analysis. They can be categorized into oracle-based (Thorup & Zwick, 2004; Baswana & Kavitha, 2006), landmark-based (Potamias et al., 2009; Sarma et al., 2010; Gubichev et al., 2010) and learning-based (Rizi et al., 2018; Schlötterer et al., 2019; Qi et al., 2020) SP representation methods. Among these categories, learning-based methods are of high accuracy and short response time (see Table 1), owing much to the flexibility of node embeddings in a metric space.

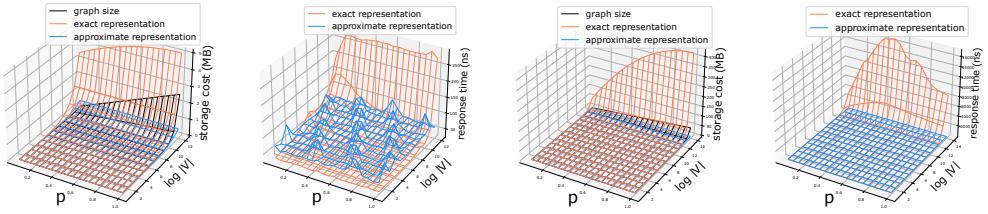

(a) (b) (c) (d)

Figure 1: Differences between approximate (ours.) and exact (PLL (Akiba et al., 2013), an efficient implementation of the hub-labeling method) SP representation methods regarding storage cost (megabytes, MB) and response time (nanoseconds, ns). We simulate a group of Bernoulli random graphs with $|V|$ nodes, and each edge is filled independently with probability p. **(a)** and **(c)** show the storage cost of exact representations increases dramatically when compared with the graph size. **(b)** and **(d)** reflect the deficiency of exact methods in response time induced by random access to massive information.

Table 1: Overall comparison of approaches to SP representation on DBLP dataset (A.7.4). PTC denotes preprocessing time complexity, PSC denotes preprocessing space complexity, RTC denotes response time complexity, TSC denotes the total storage cost for answering online distance queries, RT denotes real response time, and AL denotes accuracy loss which is measured by mRE (see Equation 1). N denotes the number of nodes in the graph, $\bar{L}(N)$ denotes the average label size of each node which increases along with N, $\bar{D}$ denotes the amortized degree on each node. α, L, n, d, w, l and β are hyperparameters in corresponded models.

Categories	Method	PTC	PSC	RTC	TSC	RT	AL
Hub-Labelling	PLL (Akiba et al., 2013)	$O(N^{1+\log \bar{L}(N)})$	$O(N\bar{L}(N))$	$O(\bar{L}(N))$	611.2 MB	2104.4 ns	-
Oracle-based	ADO (Thorup & Zwick, 2004)	$O(\alpha N^{1+\frac{1}{\alpha}})$	$O(\alpha N^{1+\frac{1}{\alpha}})$	$O(\alpha)$	5,980 MB	8,598 ns	0.4985
Landmark-based	LS (Potamias et al., 2009)	$O(lN)$	$O(lN)$	$O(l)$	334.6 MB	12,094 ns	0.3939
Learning-based	Orion (Xiaohan et al., 2010)	$O(n^2+nN)$	$O(dN)$	$O(d)$	**19.35 MB**	82.25 ns	1.1897
	Rigel (Xiaohan et al., 2011)	$O(n^2+nN)$	$O(dN)$	$O(d+\bar{D})$	35.37 MB	5,657 ns	1.0662
	DADL (Rizi et al., 2018)	$O((\lvert L\rvert+wl)N)$	$O(dN)$	$O(d+\bar{D})$	35.37 MB	7,562 ns	0.2016
	Path2Vec (Kutuzov et al., 2019)	$O((\lvert L\rvert+wl)N)$	$O(dN)$	$O(d+\bar{D})$	35.37 MB	7,700 ns	0.6097
	HALK (Schlötterer et al., 2019)	$O((\lvert L\rvert+wl)N)$	$O(dN)$	$O(d+\bar{D})$	35.37 MB	7,704 ns	0.3077
	BCDR (ours.)	$O((\lvert L\rvert+\frac{wl}{\beta})N)$	$O(dN)$	$O(d+\bar{D})$	35.37 MB	7,646 ns	**0.1712**
	BCDR-FQ (ours.)	$O((\lvert L\rvert+\frac{wl}{\beta})N)$	$O(dN)$	$O(d)$	**19.35 MB**	**58.82 ns**	0.1840

Several competitive works in learning-based methods (Rizi et al., 2018; Schlötterer et al., 2019) heuristically leverage truncated random walk and optimization of node-cooccurrence likelihood on the arbitrary linkage to learn SP representations, which achieve the state-of-the-art performance on approximation quality. However, they are not without limitations on efficiency and interpretability. On one side, a random walk is an *unstrained* node sequence from the root, possessing a limited exploration range of distance, thus resulting in uncaught distance relation with remote nodes. This is because each transition on nodes is not implied for a specific direction to move towards or beyond the root, especially after several walk steps, which restricts it from visiting remote nodes under limited walk steps (see Figure 2a). On the other side, the optimization on arbitrary linkage reflects excessively versatile local similarity among nodes, which preserves inaccurate distance relations from original graphs to the embedding space. In fact, it exerts a too-general metric over nodes' correlation, wherein the more edges or paths exist between two nodes, the stronger correlation they share. That means there are many ways to simulate a strong correlation for two nodes (e.g., add mutual edges, delete an edge to other nodes) even if some of the operations do not influence their actual SP distance (see Figures 2c and 2d). A detailed statement of related works on SP representation can be found in Appendix A.1.

In this paper, we address the above shortcomings by proposing an efficient and interpretable SP representation method called Betweenness Centrality-based Distance Resampling (BCDR). It improves the approximation quality of SP representations with two components. The first is *betweenness centrality (BC)-based random walk* to explore a wider range of distance correlation on the graph due to its awareness of high-order path structures. To the best of our knowledge, there is no exist-

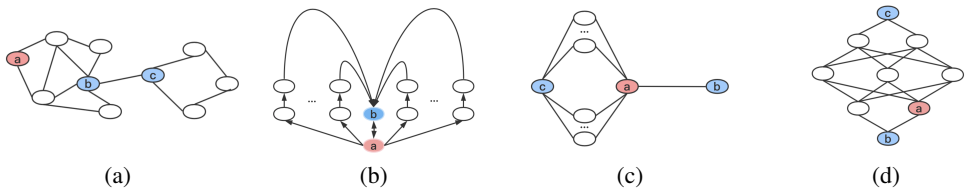

Figure 2: Distance confusion in previous SP representation learning. **(a)** random walk from v_a has much difficulty in exploring beyond current community to v_c. **(b):** node similarity on random paths misleads the measurement of SP distance since the walk from v_a is prone to steer clear of v_b for starters and back to v_b as the end, causing an extremely weak correlation between v_a and v_b even though they have an immediate edge. **(c):** a sufficient number of 2-hop links between v_c and v_a induce a shorter distance in embedding space than that of v_b and v_a. **(d):** v_b and v_c sharing substantial connection are mapped closed to each other even if they have a large SP distance gap, while the divergence of distance between v_b, v_c and v_a is also plagued with extraction.

ing method that combines betweenness centrality and random walk to learn graph representations. We prove that BC-based transition is prone to jump out of local neighborhoods compared to random transition. The second is *distance resampling* to preserve SP distance relations via implicitly decomposing an SP distance-based similarity matrix. In essence, it simulates the observation of random SPs from original walk paths and exerts desirable constraints on node representations to preserve distance relations over the graph.

We summarize our major contributions as follows. i) We propose *BC-based random walk* as an efficient strategy for exploring a wider range of SP distance within limited walk steps (see Section 3.1). ii) We propose *distance resampling* to preserve distance relations among nodes to learn an interpretable SP representation (see Section 3.2). iii) We evaluate BCDR with a broad class of real-world and synthetic graphs with diverse structures and sizes, and it yields an average improvement of 30% accuracy and 25-30% query speed, compared to all existing approximate methods for SP distance queries (see Section 4).

2 Preliminary

2.1 Notation

$G = (V, E)$ denotes an undirected graph, with $V = \{v_i\}$ being the set of nodes and $E = \{(v_i, v_j)\}$ being the set of undirected edges, and $N = |V|,\ M = |E|$. We use $Z_{N\times d}$ to represent an matrix comprising embedded vectors of nodes, where d is the embedding size, and the i-th row of Z is corresponded with v_i. Generally, for any matrix B, the symbol $\mathbf{B}_i$ represents the i-th row of B, and B_{ij} represents the element at i-th row and j-th column. A path p_{ij} of length $l \in \mathbb{N}_+$ on graph G is an ordered sequence of nodes $(v_i, v_{a_1}, \cdots, v_{a_{l-1}}, v_j)$, where each node except the last one has an edge with the subsequent node. The shortest path $\mathring{p}_{ij}$ is one of the paths with the minimum length D_{ij} between v_i and v_j. Also, the SP distance matrix D comprises $\{D_{ij}\}$. A node v_i's neighborhood $\mathcal{N}_i$ is a set of nodes with an edge with v_i, i.e., $\mathcal{N}_i = \{v_j | (v_i, v_j) \in E\}$. For high-order neighborhoods of v_i, $\mathcal{N}_i^h$ is defined as a set of nodes h-hop away from v_i, i.e., $\{v_j | D_{ij} = h\}$. A truncated random walk $\mathcal{W}_i$ rooted at node v_i of length l is a random vector of $\langle \mathcal{W}_i^1, \mathcal{W}_i^2, \cdots, \mathcal{W}_i^l \rangle$, where $\mathcal{W}_i^k$ is a node chosen from the neighborhood of node $\mathcal{W}_i^{k-1}$ for $k = 1, ..., l$, with the initial probability distribution $\mathbb{P}\{\mathcal{W}_i^0 = v_i\} \equiv 1$. W_i is a categorical distribution of nodes on $\mathcal{W}_i$, and the probability of each node in W_i represents the frequency of occurrence on the sampled paths.

2.2 Problem Definition & Metrics

The evaluation of approximate SP representation methods is divided into two stages. For the offline stage, the processing time and memory usage when constructing SP representations are evaluated, and the storage size of such representations is considered. For the online stage, the approximation quality, memory usage and query speed are evaluated. Thereinto, the commonly used metrics of

approximation quality are mean of relative error (mRE) and mean of absolute error (mAE). For a group of SP distance queries $Q = \{(v_i, v_j)\}$, mRE is defined as the relative loss of the estimated value $\tilde{D}_{ij}$ with respect to the real value D_{ij}, while mAE measures the absolute gap between them, i.e.,

$$\text{mRE} := \frac{1}{|Q|} \sum_{(v_i,v_j)\in Q} \frac{|\tilde{D}_{ij} - D_{ij}|}{D_{ij}} \qquad \text{mAE} := \frac{1}{|Q|} \sum_{(v_i,v_j)\in Q} |\tilde{D}_{ij} - D_{ij}| \tag{1}$$

For the evaluation of query speed, a million times of query requests for arbitrary pairs of nodes are performed, and the average response time for each node pair is recorded.

3 METHOD

Although random walk (RW) is universally accepted as an efficient serialization strategy of similarity measurement on graphs (Grover & Leskovec, 2016; Zhuang & Ma, 2018), we argue that the intuitive practice of RW in representing SP structures has several limitations. Consider a walk path $p = (v_a, v_{a_1}, v_{a_2}, \cdots, v_{a_l}) \in P_a$ sampled by stochastic selection on neighborhoods from root node v_a. Distance measured along p is not consistent with that on the graph (see Figure 2b) since the node sequence is *unstrained*, i.e., for $v_{a_i}, v_{a_j} \in p$, $i \leq j \not\Leftrightarrow D_{aa_i} \leq D_{aa_j}$, where i and j are indices of node v_{a_i} and v_{a_j} on p, and $1 \leq i, j \leq l$. Therefore, using the aforementioned walk paths for maximizing co-occurrence likelihood incurs two problems.

1. **Problem 1: Limited exploration range of distance**. The exploration range of rooted random walk is not in proportion to its length since each transition on the walk has an agnostic tendency to move towards or beyond the root after a few steps (see Figure 2a).
2. **Problem 2: Intractability of distance relations on paths**. The distance measured on walk paths may not actually reflect the SP distance on the graph because of the unbalanced number of links between different nodes (see Figure 2c and 2d).

In this section, we describe in detail our method as a decent way of representing SP structures. We discuss two techniques named *BC-based random walk* and *distance resampling* to address the above problems, respectively, and present the corresponding theoretical analysis for their interpretability. A time and space-efficient implementation of BCDR to integrate these techniques is available in Appendix A.2.

3.1 BC-BASED RANDOM WALK FOR WIDER EXPLORATION RANGE OF DISTANCE

Definition 1. *(Betweenness Centrality) Define $G = (V, E)$ as undirected graph. v_i, v_s, v_t are arbitrary nodes in V. $\sigma_{st}(v_i)$ represents the number of shortest paths between v_s and v_t that pass v_i, and σ_{st} is the total number of shortest paths between v_s and v_t. Then we say that BC of v_i is*

$$\text{BC}(v_i) = \sum_{s\neq i\neq t} \frac{\sigma_{st}(v_i)}{\sigma_{st}} \tag{2}$$

To address Problem 1, we propose *BC-based random walk*. As defined in Definition 1, $\text{BC}(v_i)$ determines the probability of v_i located on SPs of arbitrary node pairs. Thus, we consider a node with a large BC value vitally significant to drive the walk to move away from the root node, since it reveals an easy way of traveling to some other nodes with minimal steps. And to leverage this property, in BC-based random walk $\mathcal{W}_a = \langle \mathcal{W}_a^1, \mathcal{W}_a^2, ...\mathcal{W}_a^j, ...\rangle$ on node v_a, we prefer choosing nodes with the largest BC values among their neighborhoods when simulating walk paths, i.e.,

$$\tilde{P}(\mathcal{W}_a^j = v_j | \mathcal{W}_a^{j-1} = v_{j-1}) = \frac{\text{BC}(\mathcal{W}_a^j)}{\sum_{v_k\in\mathcal{N}_{j-1}} \text{BC}(v_k)},\ v_j \in \mathcal{N}_{j-1} \tag{3}$$

where $\tilde{P}(\cdot)$ denotes a probability distribution.

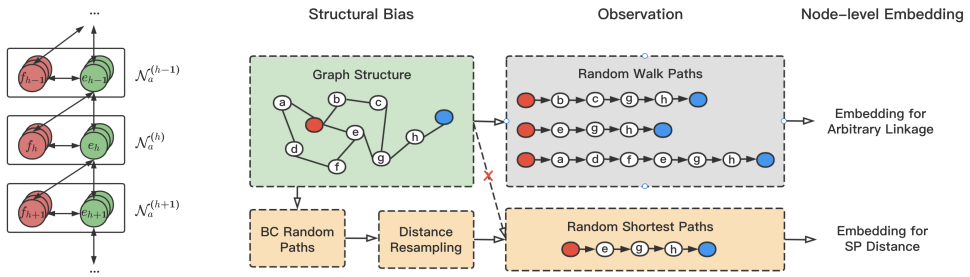

(a) (b)

Figure 3: **(a):** high-order neighborhoods' structure of v_a. *BC-based random walk* enhances the transition from f_h to e_h and e_h to e_{h+1}, prone to jump out of local neighborhoods. **(b):** comparison between general RW-based graph learning and BCDR. *Distance resampling* transforms the observation into random shortest paths, which exerts desirable constraints on learning SP representations.

Theorem 2, proved in Appendix A.3, indicates that *BC-based random walk* is prone to transit from $\mathcal{N}_a^{(h)}$ to $\mathcal{N}_a^{(h+1)}$, leading to a wider exploration range measured by the intrinsic graph's SP distance. Specifically, for each node v_a, $\mathcal{N}_a^{(h)}$ comprises two components, i.e., *final nodes* $f_h(v_a)$ and *connective nodes* $e_h(v_a)$. Thereinto, nodes in $f_h(v_a)$ have zero edge with $\mathcal{N}_a^{(h+1)}$, while nodes in $e_h(v_a)$ has several edges with $\mathcal{N}_a^{(h+1)}$, as illustrated in Figure 3a. Our method significantly improves the performance when the number of *final nodes* $|f_h(v_a)|$ is larger or there are more edges from $f_h(v_a)$ to $e_h(v_a)$ (see analysis in Remark 1).

Practically, pre-computing BC value on each node is time-consuming, which takes at least $O(NM)$ time. To address this problem, we estimate BC by leveraging breadth-first search (BFS) from a fixed number of landmarks, since nodes with large BC values tend to be visited first by BFS from any landmark. We show in Algorithm 1 and Appendix A.2.1 that this process could be involved in the simulation of distance triplets without introducing extra time complexity.

Finally, we conclude that *BC-based random walk* is a competitive walking pattern regarding exploration range of SP distance, since it possesses a strong tendency to jump out of local neighborhoods. We further verify our conclusion by comparing it with existing RW techniques in Section 4.3.

3.2 Distance Resampling for SP Distance Preservation

To address Problem 2, we propose *distance resampling*. We first illustrate a general RW-based graph learning paradigm in Figure 3b and clarify the differences between ours and other approaches. The basic idea of RW-based methods is to learn node-level embeddings Z from pieces of *observation* (i.e., walk paths), and Z thus reflects the structural bias on graphs. Specifically, for the naive RW strategy and its variants utilized in other approaches, the *observation* is a set of stochastic paths reflecting the property of arbitrary linkage between nodes, which asks Z to preserve point-wise mutual information (PMI) similarity (proved in Levy & Goldberg (2014); Shaosheng et al. (2015)). Unfortunately, the PMI similarity shares no direct connection with SP distance and causes the problems depicted in Figure 2c and 2d. To fit Z with correct information about SP structures, we intend to observe random shortest paths instead. This practice is feasible since the SP problem always has *optimal substructures*, i.e., the subpath between two nodes on any SP could also be extracted as an SP between these nodes. However, the prohibitive complexity of computing all pairs of SPs forbids us from performing such sufficient observation. By way of an alternative, we propose a resampling strategy to transform BC-based walk paths into approximate random SPs with efficient linear processing time.

Initially, we formulate the SP representation problem from the RW-based learning perspective. To avoid confusion with the symbol of paths defined above, we always use $\tilde{P}(\cdot)$ to represent a probability distribution. Let $\mathring{\mathcal{W}}_i$ and $\mathcal{W}_i$ denote random SP walk and *BC-based random walk*, respectively. We have the optimization objective on SPs, i.e., $\mathcal{L}(Z) = \mathbb{E}_{v_i \in \tilde{P}(V)} \left[\log \tilde{P}_{\mathring{W}_i | \mathbf{Z}_i}(\mathring{W}_i | \mathbf{Z}_i) \right]$. To re-

duce the complexity when optimizing on Z, we replace the probability normalization by negative sampling, according to Mikolov et al. (2013a;b), i.e.,

$$\mathcal{L}_n(Z) = \sum_{v_i \in V} \tilde{P}(v_i) \left\{ \mathbb{E}_{v_j \sim \tilde{P}_{\mathring{W}_i}(V)} [\log \sigma(\mathbf{Z}_i \mathbf{Z}_j^T)] + \lambda \mathbb{E}_{v_k \sim \tilde{P}_n(V)} [\log \sigma(-\mathbf{Z}_i \mathbf{Z}_k^T)] \right\} \tag{4}$$

, since we prefer an informative Z instead of the accurate probability. Thereinto, $\tilde{P}_n$ is the distribution of negative sampling over the graph, and λ denotes the number of negative samples. It is notable that $\mathring{W}_i$ on each node v_i is backbreaking to extract, since it requires a traversal on all SPs passing through v_i. To address this, we construct a distribution $\tilde{Q}_{W_i}$ resampled from $\tilde{P}_{W_i}$, as an efficient approximation to $\tilde{P}_{\mathring{W}_i}$, i.e.,

$$\tilde{Q}_{W_i}(v_j) = \frac{\alpha^{D_{ij}} \mathrm{BC}(v_j)}{\sum_{v_k \in W_i} \alpha^{D_{ik}} \mathrm{BC}(v_k)} \tag{5}$$

where α is a hyper-parameter controlling the weight decay by the distance, $0 < \alpha < 1$.

Finally, we maximize the following approximate objective $\hat{\mathcal{L}}_n$ instead of $\mathcal{L}_n$, i.e.,

$$\hat{\mathcal{L}}_n(Z) = \sum_{v_i \in V} \tilde{P}(v_i) \left\{ \mathbb{E}_{v_j \sim \tilde{Q}_{W_i}(V)} [\log \sigma(\mathbf{Z}_i \mathbf{Z}_j^T)] + \lambda \mathbb{E}_{v_k \sim \tilde{P}_n(V)} [\log \sigma(-\mathbf{Z}_i \mathbf{Z}_k^T)] \right\} \tag{6}$$

We show in Proposition 1 that optimization of Equation 6 conforms to implicitly decompose an SP distance-based similarity matrix where for any nodes v_a and v_b that are located far away from each other under the SP metric (i.e., a small D_{ab}) should be mapped with low similarity in the embedding space (i.e., a large $|\hat{D}_{ab}|$). Also, further discussion in Remark 2 shows that such similarity matrix $\hat{D}$ shares strong connections with the real SP distance matrix D on graphs.

Proposition 1. *Let G be an undirected graph, W_i be the multiset of nodes on the paths sampled by BC-based random walk. Negative sampling on each node v_i takes a uniform distribution on W_i. Then, for sufficient observation from $W_1, \cdots, W_N$, maximizing $\hat{\mathcal{L}}_n$ defined by Equation 6 with embeddings Z is equivalent to decomposite an SP distance-based similarity matrix $\hat{D} = ZZ^T$, where for any v_a and v_b, the distance between them in the embedding space varies linearly with respect to distance D_{ab}, namely,*

$$\hat{D}_{ab} = Z_a Z_b^T = -\log \epsilon + D_{ab} \log \alpha \tag{7}$$

where ϵ is a small constant related to the negative samples,which is independent of v_b, and α is the hyper-parameter defined in Equation 5, where $0 < \alpha < 1$.

Proposition 1 is proved in Appendix A.4.

Then, we consider the preservation of SP distance relations. Some studies on metric learning (Hermans et al., 2017; Zeng et al., 2020) have revealed that a triplet of samples (v_a, v_b, v_c) being easy to learn means if v_b shares strong correlation with v_a, the distance between v_b and v_a in the embedding space should be shorter than that of v_c and v_a. With this property, we have the following theorem, which indicates that our method is consistent with distance relations under the intrinsic SP metric.

Theorem 1. *Each symbol here follows the definition in Proposition 1. Let D be a global distance matrix defined on graph G and D_{ab} be graph's SP distance between node v_a and v_b. Then for any nodes $v_a, v_b, v_c \in G$,*

$$(D_{ab} - D_{ac})(\hat{D}_{ab} - \hat{D}_{ac}) \leq 0 \tag{8}$$

The proof is presented in Appendix A.6.

In conclusion, we discuss here the significance of *distance resampling* for preserving distance relations. It exerts two implicit constraints on Z to learn an interpretable SP representation. First, as stated in Proposition 1, the distance measured in the embedding space shares a strong negative correlation with that measured on the graph. Second, for any node triplet, the distance relation between any two of them is preserved according to Theorem 1. The two constraints are further verified in Section 4.3 against existing techniques.

3.3 EFFICIENT IMPLEMENTATION OF BCDR ALGORITHM

We also provide a time and space-efficient implementation of BCDR to integrate the above techniques in Algorithm 1. Like previous learning-based SP representation methods, we first transform the graph into low-dimensional embeddings (i.e., $Z_{N\times d}$) and learn a distance predictor $g_\phi : (\mathbb{R}^d, \mathbb{R}^d) \to \mathbb{R}$ by observed distance triplets $\{(\mathbf{Z}_a, \mathbf{Z}_b, D_{ab})\}$. Finally, the predictor g_ϕ will be involved in answering online distance queries. We describe the detailed designs of these procedures in Appendix A.2.

4 EXPERIMENTAL EVALUATION

In this section, we show the comprehensive performance of BCDR with 5 real-world graphs of different sizes and 6 synthetic graphs of different structures. Specifically, we evaluate BCDR on 3 small graphs (i.e., Cora, Facebook and GrQc) and 2 large graphs (i.e., DBLP and Youtube) for its scalability (see Section 4.2), and evaluate it on 6 synthetic graphs for its representational capacity of complex structures (see Section 4.3 and 4.4). Our method is compared with strong baselines from both approximate SP representation and general graph representation learning (GRL). In the experiments, we also provide two variants of BCDR, i.e., BCDR-FC and BCDR-FQ, for accelerating the construction and querying process, respectively. A detailed description of the datasets, including statistics and visualization, is thoroughly provided in Appendix A.7.

4.1 BASELINE & PARAMETER SETUP

The parameter setups of each baseline are listed as follows. For the oracle-based method, α is set to 2 for the best accuracy, as discussed in the previous work. For the landmark-based method, we choose a sufficient size of the landmark set as $|L| = 128$ and take the constrained strategy, i.e., for each landmark selected, nodes within two hops are discarded from consideration. For learning-based methods, the embedding sizes d are fixed at 80 for small graphs (i.e., Cora, Facebook, and GrQc) and 24 for large graphs (i.e., DBLP and Youtube). Other hyper-parameters of each model follow the default configurations discussed in their works. For general GRL methods, all of the baselines follow the default configurations and are further trained by linear regression to extract the distance between any two nodes.

For our proposed method, we simulate $w_{in} = 20$ walks on each node, and each walk is truncated at a length of $l_{in} = 40$. Each landmark is selected randomly up to the size of a landmark set $|L| = 16$. The number of negative samples n is set to 1. The process of distance resampling outputs $w_{out} = 40$ walks with each walk at a length of $l_{out} = 10$. The decay coefficients of BC and distance are fixed as $\zeta = 10,\ \mu = 0.35$. We train the distance predictor using a two-layer perceptron with a learning rate $\epsilon_r = 0.01$. The training process takes a total of 15 epochs. For large graphs (i.e., DBLP and YouTube), we adjust the above parameters by $|L| = 5, w_{in} = 2,\ \zeta = 1.0$. For BCDR-FC, the number of walks is reduced by a half for every graph. For BCDR-FQ, we take the raw outputs of the distance predictor without searching first-order neighborhoods on the graph (i.e., set $\tau = \mathrm{True}$).

All of the above models are run with six 3.50GHz Intel Xeon(R) CPUs and 128GB memory, and the precomputed representations of each model are serialized by Pickle.

4.2 PERFORMANCE OF APPROXIMATE SP DISTANCE QUERY

We compare BCDR with other learning-based SP representation methods (i.e., Orion (Xiaohan et al., 2010), Rigel (Xiaohan et al., 2011), DADL (Rizi et al., 2018), Path2Vec (Kutuzov et al., 2019) and HALK (Schlötterer et al., 2019)) as well as other approximate methods, including landmark-based (i.e., LS (Potamias et al., 2009) and oracle-based (i.e., ADO (Thorup & Zwick, 2004)) techniques. Like previous works, we initially compute all pairs of SP distance on each real-world graph by BFS and take a uniform sampling to select a group of one million distance triplets $\{(v_a, v_b, D_{ab})\}$ as test samples. All of the baselines, including ours, are purely implemented in Python 3.9 and evaluated under the same environment. Since only unweighted graphs are considered, the outputs of each model are quantized to integer when evaluating accuracy loss. Some of the experimental results are shown in Table 2 (see Appendix A.8 for extended results on other graphs and comparisons with GRL

models). We can see from the table that our model not only outperforms previous models regarding accuracy loss for all graphs but also shares competitive results on other metrics.

In detail, for *accuracy loss* (mAE and mRE), BCDR answers arbitrary queries with the minimum error due to a wider exploration range of distance and distance-preserved optimization. The result also reveals that RW-based approaches (DADL, HALK, and BCDR) achieve higher accuracy than others. For *offline processing time* (PT), *memory usage* (PMU), and *storage cost* (SC), the results show BCDR possesses powerful scalability against the growth of graph scale. Even for a graph with millions of nodes, the offline processing could be completed within several hours, and the memory usage is close to the graph size. This is because we perform truncated random walks with a fixed length on every graph, and the size of walk data is further reduced by the distance resampling strategy. For *response time* (RT) and *memory usage* (QMU) in querying, we see all learning-based models share similar memory usage since each distance query could be answered by checking the node embeddings and graph adjacency matrices. BCDR-FQ and Orion could answer such a query within tens of nanoseconds due to the absence of double-checking on adjacency matrices.

Table 2: Performance comparison of approximate methods on SP distance representations. PT denotes processing time when constructing SP representations, PMU denotes memory usage in such processing, SC denotes space cost on storing SP representations, RT denotes average response time of answering a distance query, QMU denotes memory usage in the querying stage, mAE and mRE are the metrics of accuracy loss. DNF means it did not finish in one day.

Dataset	Model	PT	PMU	SC	RT	QMU	mAE	mRE
DBLP	ADO	37,029 s	8,899 MB	199.8 MB	8,598 ns	5,980 MB	3.0691	0.4985
	LS	5,838 s	349.0 MB	80.02 MB	12,094 ns	344.6 MB	2.5060	0.3939
	Orion	5,531 s	321.8 MB	**19.36 MB**	**82.25 ns**	**19.35 MB**	3.5044	0.5165
	Rigel	5,523 s	321.8 MB	**19.36 MB**	**5,657 ns**	**35.37 MB**	3.5043	0.5164
	DADL	2,650 s	1,958 MB	**19.36 MB**	7,562 ns	**35.37 MB**	**1.2753**	0.2016
	Path2Vec	27,453 s	140.9 MB	**19.36 MB**	7,700 ns	**35.37 MB**	3.9474	0.6097
	HALK	1,270 s	649.6 MB	**19.36 MB**	7,704 ns	**35.37 MB**	1.8477	0.3077
	BCDR (ours.)	**1,086 s**	**53.52 MB**	**19.36 MB**	7,646 ns	**35.37 MB**	**1.1857**	**0.1712**
	BCDR-FQ (ours.)	**1,026 s**	**53.52 MB**	**19.36 MB**	**58.82 ns**	**19.35 MB**	1.3018	**0.1840**
	BCDR-FC (ours.)	**999.8 s**	**53.52 MB**	**19.36 MB**	7,617 ns	**35.37 MB**	**1.1014**	**0.1580**
Youtube	ADO	DNF	–	–	–	–	–	–
	LS	87,902 s	1,258 MB	286.7 MB	16,672 ns	1,217 MB	2.0159	0.4091
	Orion	50,484 s	1,251 MB	**69.26 MB**	**163.9 ns**	**69.26 MB**	2.8642	0.5473
	Rigel	51,246 s	1,251 MB	**69.26 MB**	13,808 ns	**114.9 MB**	2.8642	0.5473
	DADL	28,351 s	6,983 MB	**69.27 MB**	7,708 ns	**114.9 MB**	1.1144	0.2163
	Path2Vec	DNF	–	–	–	–	–	–
	HALK	**5,971** s	2,187 MB	**69.27 MB**	7,764 ns	**114.9 MB**	1.9035	0.3860
	BCDR (ours.)	**7,794 s**	**179.8 MB**	**69.27 MB**	7,585 ns	**114.9 MB**	**0.9080**	**0.1677**
	BCDR-FQ (ours.)	7,893 s	**179.8 MB**	**69.27 MB**	**63.78 ns**	**69.27 MB**	**0.9004**	**0.1704**
	BCDR-FC (ours.)	**6,000 s**	**179.8 MB**	**69.27 MB**	**6,156 ns**	**114.9 MB**	**0.9083**	**0.1745**

4.3 Exploration Range of Distance

As stated in Section 3.1, the exploration range of distance could be widened by *BC-based random walk* (BC-RW), which helps to model high-order correlation by SP distance. Here, we compare BC-RW with existing renowned walk strategies, including naive random walk (NRW) (Perozzi et al., 2014; Zhuang & Ma, 2018), second-order random walk (SORW) (Grover & Leskovec, 2016), random surfing (RS) (Cao et al., 2016). We also consider a DFS-like random walk (DFS-RW) as a strong baseline by setting a very small q in Node2Vec for deep exploration. The methods are tested on 6 synthetic graphs with divergent structures. We randomly sample 20 root nodes and, for each root, simulate 10 walks to show how many nodes with different distance are explored at each step of the walk. The ideal situation for rooted walk paths with a fixed length l is to cover up to nodes l-hop away from the current root. The results on *circle graphs* are shown in Figure 4. We can see from the results that our proposed BC-RW is much more competitive in exploring a wider range of SP distance. Further results and analysis on different graph structures are presented in Appendix A.9.

4.4 Preservation of Distance Relations

As discussed in Section 3.2, *distance resampling* is proposed to preserve distance relations via implicitly decomposing an SP distance-based similarity matrix. Here, we show its interpretability for SP representations by visualizing the properties of embedded vectors Z when compared with the maximum likelihood optimization on other biased random walks. Environment configuration follows the previous section.

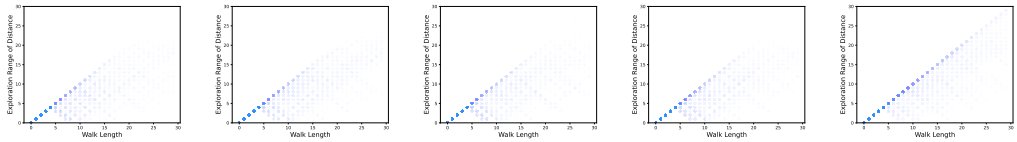

Figure 4: Exploration range of distance when taking different walk strategies on *circle graphs*. **Column from left to right:** different walk strategies including NRW, SORW, RS, DFS-RW, BC-RW (ours.), respectively.

First, we evaluate the relation of distance measured on graphs and embedding spaces for each node pair. Specifically, distance on the embedding space is measured by inner product $\mathbf{Z}_i\mathbf{Z}_j^T$ for given nodes v_i and v_j, and that on the graph is measured by SP distance. Initially, we learn embedded vectors from walk paths simulated by each walk strategy and randomly sample 100 source nodes with 100 destinations for each source. The results on *circle graphs* are shown in Figure 5 (refer to Appendix A.10 for extended results on other graphs), which indicates that embeddings enhanced by *distance resampling* have a better tendency to maintain a linear relationship on the distance metric between the original graph and embedding space. The results also verified our analysis in Remark 2 regarding relations between the SP distance-based similarity matrix $\hat{D}$ and the distance matrix D.

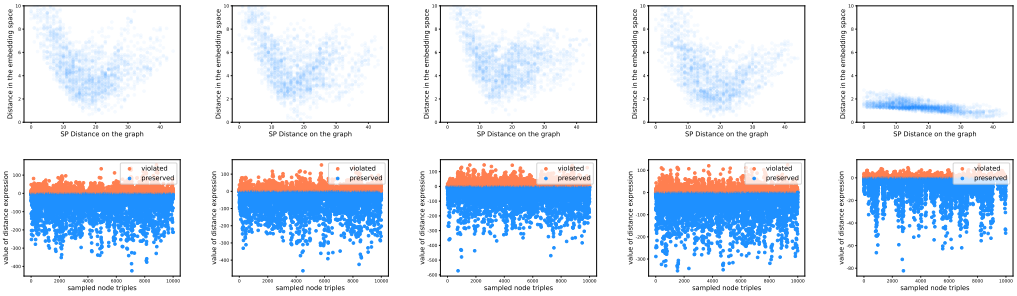

Figure 5: **Row 1:** measured distance from the embedding space and the original graph. **Row 2:** whether distance relations are violated in the embedding space. **Columns from left to right:** embeddings learned by different walk strategies,i.e., NRW, SORW, RS, DFS-RW, and BC-RW (ours.), respectively. For ours, walk paths are further simulated by *distance resampling*.

Second, we try to find out how much the probability distance relation is violated in the embedding space, i.e., whether a pair of nodes with larger SP distance is corresponded with less embedded similarity as described in Theorem 1. We randomly take $10,000$ node triplets $\{(v_a, v_b, v_c)\}$, and record if Equation 8 is satisfied. The results on *circle graphs* are shown in Figure 5 (refer to Appendix A.10 for extended results on other graphs). The figure confirms that our model is much more satisfactory in preserving distance relation than existing methods. This is because BC-RW provide sufficient observation on each node by locating many distant nodes with a sequence of centralized nodes on a graph, and thus *distance resampling* based on such observation could preserve distance relations of each node within its exploration range.

5 Conclusion

In this paper, we propose a novel graph SP representation method called Betweenness Centrality-based Distance Resampling (BCDR) and discuss two significant techniques for an efficient and interpretable SP representation. The experimental evaluation indicates that BCDR improves the approximation quality with a shorter response time for SP Distance queries and possesses strong scalability to large-scale and complex graphs. Its node representations also reflect the highly-efficient paths for high-order message passing in graph neural networks, which appears to be helpful for structural graph pooling and inference. This will be our future work.

REFERENCES

A. Ahmed, N. Shervashidze, S. Narayanamurthy, V. Josifovski, and A. J. Smola. Distributed large-scale natural graph factorization. In *Proceedings of the 22nd international conference on World Wide Web*, pp. 37–48, 2013.

Takuya Akiba, Yoichi Iwata, and Yuichi Yoshida. Fast exact shortest-path distance queries on large networks by pruned landmark labeling. In *Proceedings of the 2013 ACM SIGMOD International Conference on Management of Data*, pp. 349–360, 2013.

Muhammad Asif, Hassan Raza, and Muhammad Imran Manzoor. A novel approach for tenuous community detection in social networks. *International Journal of Data Analytics (IJDA)*, 3(1): 1–12, 2022.

Egon Balas. Tutorial paper x: A class of location, distribution and scheduling problems: modelling and solution methods. *JORBEL-Belgian Journal of Operations Research, Statistics, and Computer Science*, 22(2):36–69, 1982.

S. Baswana and T. Kavitha. Faster algorithms for approximate distance oracles and all-pairs small stretch paths. In *2006 47th Annual IEEE Symposium on Foundations of Computer Science (FOCS'06)*, pp. 591–602, Oct 2006. doi: 10.1109/FOCS.2006.29.

Shaosheng Cao, Wei Lu, and Qiongkai Xu. Deep neural networks for learning graph representations. In *Proceedings of the AAAI Conference on Artificial Intelligence*, volume 30, 2016.

Jason Carlton. The shortest distance between two people is a story: Storytelling best practices in digital and social media marketing. *Journal of Digital & Social Media Marketing*, 8(2):108–115, 2020.

Sudhanshu Chanpuriya, Cameron Musco, Konstantinos Sotiropoulos, and Charalampos Tsourakakis. Node embeddings and exact low-rank representations of complex networks. *Advances in Neural Information Processing Systems*, 33, 2020.

Haochen Chen, Bryan Perozzi, Yifan Hu, and Steven Skiena. Harp: Hierarchical representation learning for networks. In *Proceedings of the AAAI conference on artificial intelligence*, volume 32, 2018.

Wei Chen, Christian Sommer, Shang-Hua Teng, and Yajun Wang. Compact routing in power-law graphs. In *International Symposium on Distributed Computing*, pp. 379–391. Springer, 2009.

Yu Chen, Hanchao Ku, and Mingwu Zhang. Pp-ocq: A distributed privacy-preserving optimal closeness query scheme for social networks. *Computer Standards & Interfaces*, 74:103484, 2021.

Edith Cohen, Eran Halperin, Haim Kaplan, and Uri Zwick. Reachability and distance queries via 2-hop labels. *SIAM Journal on Computing*, 32(5):1338–1355, 2003.

Manuel Costa, Miguel Castro, R Rowstron, and Peter Key. Pic: Practical internet coordinates for distance estimation. In *24th International Conference on Distributed Computing Systems, 2004. Proceedings.*, pp. 178–187. IEEE, 2004.

Frank Dabek, Russ Cox, Frans Kaashoek, and Robert Morris. Vivaldi: A decentralized network coordinate system. *ACM SIGCOMM Computer Communication Review*, 34(4):15–26, 2004.

Daniel Delling, Andrew V Goldberg, Thomas Pajor, and Renato F Werneck. Robust distance queries on massive networks. In *European Symposium on Algorithms*, pp. 321–333. Springer, 2014.

Mihaela Enachescu, Mei Wang, and Ashish Goel. Reducing maximum stretch in compact routing. In *IEEE INFOCOM 2008-The 27th Conference on Computer Communications*, pp. 336–340. IEEE, 2008.

Muhammad Farhan, Qing Wang, Yu Lin, and Brendan McKay. A highly scalable labelling approach for exact distance queries in complex networks. *Network*, 400(3B):8B, 2019.

Ada Wai-Chee Fu, Huanhuan Wu, James Cheng, and Raymond Chi-Wing Wong. Is-label: an independent-set based labeling scheme for point-to-point distance querying. *Proceedings of the VLDB Endowment*, 6(6):457–468, 2013.

Lucia Galovičová, Petra Borotová, Veronika Valková, Nenad L Vukovic, Milena Vukic, Jana Štefániková, Hana Ďúranová, Przemysław Łukasz Kowalczewski, Natália Čmiková, and Miroslava Kačániová. Thymus vulgaris essential oil and its biological activity. *Plants*, 10(9): 1959, 2021.

A. Grover and J. Leskovec. node2vec: Scalable feature learning for networks. In *the 22nd ACM SIGKDD International Conference*, 2016.

A. Gubichev, S. Bedathur, S. Seufert, and G. Weikum. Fast and accurate estimation of shortest paths in large graphs. In *Proceedings of the 19th ACM Conference on Information and Knowledge Management, CIKM 2010, Toronto, Ontario, Canada, October 26-30, 2010*, 2010.

Peter E Hart, Nils J Nilsson, and Bertram Raphael. A formal basis for the heuristic determination of minimum cost paths. *IEEE transactions on Systems Science and Cybernetics*, 4(2):100–107, 1968.

Alexander Hermans, Lucas Beyer, and Bastian Leibe. In defense of the triplet loss for person re-identification. *arXiv preprint arXiv:1703.07737*, 2017.

Omar Houidi, Oussama Soualah, Wajdi Louati, and Djamal Zeghlache. Dynamic vnf forwarding graph extension algorithms. *IEEE Transactions on Network and Service Management*, 17(3): 1389–1402, 2020.

Shijie Jiang, Yang Wang, Guang Lu, and Chuanwen Li. Dlsm: Distance label based subgraph matching on gpu. In *Asia-Pacific Web (APWeb) and Web-Age Information Management (WAIM) Joint International Conference on Web and Big Data*, pp. 194–200. Springer, 2021.

Andrey Kutuzov, Mohammad Dorgham, Oleksiy Oliynyk, Chris Biemann, and Alexander Panchenko. Making fast graph-based algorithms with graph metric embeddings. In *Proceedings of the 57th Annual Meeting of the Association for Computational Linguistics*, pp. 3349–3355, Florence, Italy, July 2019. Association for Computational Linguistics. doi: 10.18653/v1/P19-1325. URL `https://aclanthology.org/P19-1325`.

James R Lee. Volume distortion for subsets of euclidean spaces. *Discrete & Computational Geometry*, 41(4):590–615, 2009.

Sanghwan Lee, Zhi-Li Zhang, Sambit Sahu, and Debanjan Saha. On suitability of euclidean embedding of internet hosts. *ACM SIGMETRICS Performance Evaluation Review*, 34(1):157–168, 2006.

Jure Leskovec and Andrej Krevl. SNAP Datasets: Stanford large network dataset collection. `http://snap.stanford.edu/data`, June 2014.

Omer Levy and Yoav Goldberg. Neural word embedding as implicit matrix factorization. *Advances in neural information processing systems*, 27:2177–2185, 2014.

Ziyi Liu, Lei Li, Mengxuan Zhang, Wen Hua, Pingfu Chao, and Xiaofang Zhou. Efficient constrained shortest path query answering with forest hop labeling. In *2021 IEEE 37th International Conference on Data Engineering (ICDE)*, pp. 1763–1774. IEEE, 2021.

Yun Mao, Lawrence K Saul, and Jonathan M Smith. Ides: An internet distance estimation service for large networks. *IEEE Journal on Selected Areas in Communications*, 24(12):2273–2284, 2006.

Vardges Melkonian et al. Mathematical models for a social partitioning problem. *American Journal of Computational Mathematics*, 11(01):1, 2021.

Tomas Mikolov, Kai Chen, Greg Corrado, and Jeffrey Dean. Efficient estimation of word representations in vector space. *arXiv preprint arXiv:1301.3781*, 2013a.

Tomas Mikolov, Ilya Sutskever, Kai Chen, Greg S Corrado, and Jeff Dean. Distributed representations of words and phrases and their compositionality. In *Advances in neural information processing systems*, pp. 3111–3119, 2013b.

TS Eugene Ng and Hui Zhang. Predicting internet network distance with coordinates-based approaches. In *Proceedings. Twenty-First Annual Joint Conference of the IEEE Computer and Communications Societies*, volume 1, pp. 170–179. IEEE, 2002.

TS Eugene Ng and Hui Zhang. A network positioning system for the internet. In *USENIX Annual Technical Conference, General Track*, pp. 141–154, 2004.

Ruksar Parveen and N Sandeep Varma. Friend's recommendation on social media using different algorithms of machine learning. *Global Transitions Proceedings*, 2021.

B. Perozzi, R. Al-Rfou, and S. Skiena. Deepwalk: Online learning of social representations. *Proceedings of the ACM SIGKDD International Conference on Knowledge Discovery and Data Mining*, 03 2014. doi: 10.1145/2623330.2623732.

Bryan Perozzi, Vivek Kulkarni, Haochen Chen, and Steven Skiena. Don't walk, skip! online learning of multi-scale network embeddings. In *Proceedings of the 2017 IEEE/ACM International Conference on Advances in Social Networks Analysis and Mining 2017*, pp. 258–265, 2017.

Michalis Potamias, Francesco Bonchi, Carlos Castillo, and Aristides Gionis. Fast shortest path distance estimation in large networks. In *Proceedings of the 18th ACM conference on Information and knowledge management*, pp. 867–876, 2009.

Jianzhong Qi, Wei Wang, Rui Zhang, and Zhuowei Zhao. A learning based approach to predict shortest-path distances. In Angela Bonifati, Yongluan Zhou, Marcos Antonio Vaz Salles, Alexander Böhm, Dan Olteanu, George H. L. Fletcher, Arijit Khan, and Bin Yang (eds.), *Proceedings of the 23rd International Conference on Extending Database Technology, EDBT 2020, Copenhagen, Denmark, March 30 - April 02, 2020*, pp. 367–370. OpenProceedings.org, 2020. doi: 10.5441/002/edbt.2020.34. URL https://doi.org/10.5441/002/edbt.2020.34.

Jiezhong Qiu, Yuxiao Dong, Hao Ma, Jian Li, Kuansan Wang, and Jie Tang. Network embedding as matrix factorization: Unifying deepwalk, line, pte, and node2vec. In *Proceedings of the eleventh ACM international conference on web search and data mining*, pp. 459–467, 2018.

Bayu Rahmad Syah, Mahyuddin Nasution, Erna Nababan, and Syahril Efendi. Sensitivity of shortest distance search in the ant colony algorithm with varying normalized distance formulas. *TELKOMNIKA Indonesian Journal of Electrical Engineering*, 19:1251–1259, 08 2021. doi: 10.12928/TELKOMNIKA.v19i4.18872.

Satish Rao. Small distortion and volume preserving embeddings for planar and euclidean metrics. In *Proceedings of the fifteenth annual symposium on Computational geometry*, pp. 300–306, 1999.

Fatemeh Salehi Rizi, Joerg Schloetterer, and Michael Granitzer. Shortest path distance approximation using deep learning techniques. In *2018 IEEE/ACM International Conference on Advances in Social Networks Analysis and Mining (ASONAM)*, pp. 1007–1014. IEEE, 2018.

S. T. Roweis and L. K. Saul. Nonlinear dimensionality reduction by locally linear embedding. *science*, 290(5500):2323–2326, 2000.

A. D. Sarma, S. Gollapudi, M. Najork, and R. Panigrahy. A sketch-based distance oracle for web-scale graphs. In *Proceedings of the Third International Conference on Web Search and Web Data Mining, WSDM 2010, New York, NY, USA, February 4-6, 2010*, 2010.

Jörg Schlötterer, Martin Wehking, Fatemeh Salehi Rizi, and Michael Granitzer. Investigating extensions to random walk based graph embedding. In *2019 IEEE International Conference on Cognitive Computing (ICCC)*, pp. 81–89. IEEE, 2019.

Mirco Schönfeld and Jürgen Pfeffer. Shortest path-based centrality metrics in attributed graphs with node-individual context constraints. *Social Networks*, 2021.

C. Shaosheng, L. Wei, and X. Qiongkai. Grarep: Learning graph representations with global structural information. In *Proceedings of the 24th ACM international on conference on information and knowledge management*, pp. 891–900, 2015.

Yuval Shavitt and Tomer Tankel. Hyperbolic embedding of internet graph for distance estimation and overlay construction. *IEEE/ACM Transactions on Networking*, 16(1):25–36, 2008.

Marcus Sokolowski and Danuta Wasserman. A candidate biological network formed by genes from genomic and hypothesis-free scans of suicide. *Preventive Medicine*, 152:106604, 2021.

Liying Tang and Mark Crovella. Virtual landmarks for the internet. In *Proceedings of the 3rd ACM SIGCOMM conference on Internet measurement*, pp. 143–152, 2003.

M. Thorup and U. Zwick. Approximate distance oracles. *Journal of the Acm*, 52(1), 2004.

Konstantin Tretyakov, Abel Armas-Cervantes, Luciano García-Bañuelos, Jaak Vilo, and Marlon Dumas. Fast fully dynamic landmark-based estimation of shortest path distances in very large graphs. In *Proceedings of the 20th ACM International Conference on Information and Knowledge Management*, CIKM '11, pp. 1785–1794, New York, NY, USA, 2011. Association for Computing Machinery. ISBN 9781450307178. doi: 10.1145/2063576.2063834. URL https://doi.org/10.1145/2063576.2063834.

Anton Tsitsulin, Davide Mottin, Panagiotis Karras, and Emmanuel Müller. Verse: Versatile graph embeddings from similarity measures. In *Proceedings of the 2018 World Wide Web Conference*, pp. 539–548, 2018.

Z. Xiaohan, A. Sala, C. Wilson, Z. Haitao, and Z. Ben Y. Orion: Shortest path estimation for large social graphs. In *Proceedings of the 3rd Wonference on Online Social Networks*, WOSN'10, pp. 9, USA, 2010. USENIX Association.

Z. Xiaohan, A. Sala, Z. Haitao, and Z. Ben. Fast and scalable analysis of massive social graphs. *CoPR*, 07 2011.

Yiding Yang, Xinchao Wang, Mingli Song, Junsong Yuan, and Dacheng Tao. Spagan: Shortest path graph attention network. *arXiv preprint arXiv:2101.03464*, 2021.

Huilin Yuan, Jianlu Hu, Yufan Song, Yanke Li, and Jie Du. A new exact algorithm for the shortest path problem: An optimized shortest distance matrix. *Computers & Industrial Engineering*, 158: 107407, 2021.

Xiang Yue, Zhen Wang, Jingong Huang, Srinivasan Parthasarathy, Soheil Moosavinasab, Yungui Huang, Simon M Lin, Wen Zhang, Ping Zhang, and Huan Sun. Graph embedding on biomedical networks: methods, applications and evaluations. *Bioinformatics*, 36(4):1241–1251, 10 2019. ISSN 1367-4803. doi: 10.1093/bioinformatics/btz718. URL https://doi.org/10.1093/bioinformatics/btz718.

Abeer A Zaki, Nesma A Saleh, and Mahmoud A Mahmoud. Performance comparison of some centrality measures used in detecting anomalies in directed social networks. *Communications in Statistics-Simulation and Computation*, pp. 1–15, 2021.

Kaiwei Zeng, Munan Ning, Yaohua Wang, and Yang Guo. Hierarchical clustering with hard-batch triplet loss for person re-identification. In *Proceedings of the IEEE/CVF Conference on Computer Vision and Pattern Recognition*, pp. 13657–13665, 2020.

Weitong Zhang, Ronghua Shang, and Licheng Jiao. Complex network graph embedding method based on shortest path and moea/d for community detection. *Applied Soft Computing*, 97:106764, 2020.

Han Zheng, Eng Keong Lua, Marcelo Pias, and Timothy G Griffin. Internet routing policies and round-trip-times. In *International Workshop on Passive and Active Network Measurement*, pp. 236–250. Springer, 2005.

Chenyi Zhuang and Qiang Ma. Dual graph convolutional networks for graph-based semi-supervised classification. In *Proceedings of the 2018 World Wide Web Conference*, pp. 499–508, 2018.

A APPENDIX

A.1 RELATED WORK

A.1.1 APPROXIMATE SP REPRESENTATION

Hard-coding Perspective Compared with exact SP representations that improve query speed at the expense of huge storage costs, approximate methods are designed to find a compact and scalable representation of high performance both in time and space. The basic idea of these methods is to reduce the complexity of SP distance matrices. Thorup and Zwick (Thorup & Zwick, 2004) initially observe that a hierarchical sparse sampling of nodes could significantly reduce the number of elements in the distance matrix, and all pairs of SP distance are thus approximately represented by the distance relations on those nodes with a bounded error. They also provide a time-efficient algorithm to compute the pruned distance relations. Several later extensions (Baswana & Kavitha, 2006; Enachescu et al., 2008; Chen et al., 2009) are proposed to improve the processing time and space on specific graphs. However, these methods still have limitations on space complexity and accuracy. First, the sampled distance relations take $O(\alpha N^{1+\alpha})$ space which is not linear to the number of nodes N, thus inducing scalable problems on large graphs. Second, the bounded error is often unacceptable on graphs with smaller diameters since even the most accurate model (with $\alpha = 2$) allows three times the error of real distance.

Addressing these issue, landmark-based distance estimation methods (Potamias et al., 2009; Gubichev et al., 2010; Sarma et al., 2010) are proposed. Instead of sampling hierarchical sets of nodes, landmark-based methods only preserve distance relations between a fixed number of nodes (called landmarks) to others on the graph, and all pairs of SP distance could be bounded by their distance related to landmarks according to triangle inequality (Zheng et al., 2005; Lee et al., 2006; Mao et al., 2006), i.e., for any nodes v_a and v_b,

$$\max_{v_i \in L} |D_{ai} - D_{ib}| \leq D_{ab} \leq \min_{v_j \in L} |D_{ai} + D_{ib}| \tag{9}$$

where D_{ab} denotes the SP distance between v_a and v_b, L denotes the set of landmarks. The average accuracy could be optimized by selecting proper landmarks that covers SPs as many as possible. Unfortunately, finding the optimal finite set of landmarks with the minimal size has been proved to be NP-hard, which is mapping to set-cover problem (Balas, 1982). Therefore, several heuristic selection strategies are discussed to tight Equation 9 by leading D_{ab} almost near to its upper bound (Potamias et al., 2009). Other efforts (Gubichev et al., 2010; Tretyakov et al., 2011) are made to store SP trees for each landmark instead of distances at the cost of extra storage and response time. Nevertheless, the approximation performance in these models relies highly on graph structures, since less-centralized graphs (e.g., a grid-like graph) and graphs of large diameters (e.g., a large planar graph) require a large number of distributed landmarks to cover distant pairs of nodes.

Learning Perspective Instead of hard-coding techniques mentioned above, our work steps forward from a learning perspective of SP distance estimation, which constructs general and scalable representations for arbitrary graphs. Under the low-rank assumption of SP distance matrices, the basic idea of learning-based methods is to transform the graph into a metric space while preserving the distance between pairs of nodes. As the embedding space is low-dimensional and continuous, extracting distance from learning-based SP representations is fast and scalable. However, directly optimizing the distance between all pairs is time-consuming, which takes at least $O(N^2)$ time for computing distance and subsequent optimization. Towards this, many graph coordinate systems (Ng & Zhang, 2002; Tang & Crovella, 2003; Costa et al., 2004; Dabek et al., 2004; Ng & Zhang, 2004) are studied in the past years. To reduce processing complexity, a feasible learning procedure for very large graphs recently proposed in Orion (Xiaohan et al., 2010) contains three steps. First, perform breadth-first search (BFS) from a small landmark set L and record node pairs as well as their distance as training triplets $\{\langle v_l, v_a, D_{la} \rangle\}$ where $v_l \in L,\ v_a \in V$. Second, create a graph coordinate system M by preserving distance relations among nodes in L, i.e.,

$$\arg \min_{L^M = \{v_i^M | v_i \in L\}} \sum_{v_i, v_j \in L} |D_{ij}^M - D_{ij}| \tag{10}$$

where v_i^M denotes the embedded vector corresponding to the node v_i, and D_{ij}^M denotes the geodesic distance between v_i^M and v_j^M measured on M. Third, fix L^M and calibrate distance between other

nodes and landmarks iteratively. Among these steps, the metric tensor defined on M significantly affects the accuracy of distance estimation, and models regarding embedding in euclidean space (Rao, 1999; Lee, 2009; Xiaohan et al., 2010) and hyperbolic space (Shavitt & Tankel, 2008; Xiaohan et al., 2011) are well studied respectively.

Inspired by the great success in graph representation learning (GRL), further work (Rizi et al., 2018; Schlötterer et al., 2019) including ours treats M as an agnostic but definite manifold learned by GRL techniques and estimates distance based on learnable metric criteria (usually a multi-layer perceptron). Therefore, the learning task here is converted from "calibrate the position of each node" to "learn powerful metric criteria to extract distance everywhere." This novel paradigm achieves higher accuracy with reduced training time despite the fact that we are unsure about whether general GRL models could embed sufficient information to infer all pairs of SPs. In this paper, we thus discuss an interpretable SP representation learning method and improve the comprehensive performance of SP distance estimation.

A.1.2 Graph Representation Learning

Graph representation learning (GRL) organizes symbolic objects (such as nodes, edges, clusters) in a way such that their similarities on the graph are well-preserved in the low-dimensional embedding space. Currently, most of these methods focus on preserving arbitrary linkage on graphs by considering high-order adjacency matrices, and are categorized into matrix factorization (MF) and random walk (RW) approaches. Thereinto, our work shares strong connections with general RW approaches which embeds distant nodes' correlation within linear complexity compared with MF methods. The basic idea of RW-based learning methods proposed in Deepwalk (Perozzi et al., 2014) is to dump complicated linkage structure on graphs into a few fixed-length node sequences in a statistical view and learn node embeddings to reflect their co-occurrence on walk paths using a skip-gram algorithm (Mikolov et al., 2013a;b). The learning process is to solve a maximum likelihood optimization problem based on observed sequences, i.e., for any nodes v_a and v_b,

$$\arg\max_{\mathbf{Z}_a,\mathbf{Z}_b} \log\sigma(\mathbf{Z}_a\mathbf{Z}_b^T) + \lambda\mathbb{E}_{v_k\sim\tilde{P}_n(V)}[\log\sigma(-\mathbf{Z}_a\mathbf{Z}_k^T)])] \tag{11}$$

where $\mathbf{Z}_a$ denotes the embedded vector of v_a, λ denotes the number of negative samples, $\sigma(\cdot)$ denotes the sigmoid function where $\sigma(x) = (1+e^{-x})^{-1}$, and $\tilde{P}_n(\cdot)$ denotes a probability distribution of the negative sampling. Several practical strategies are proposed in the past few years to simulate structure-aware traversal on graphs in RW-based methods (Grover & Leskovec, 2016; Cao et al., 2016; Perozzi et al., 2017; Chen et al., 2018). In detail, to enhance sensibility on divergent structures, Node2Vec (Grover & Leskovec, 2016) exploits a biased random walk strategy to perform combinatorial traversal on graphs, including breadth-first search (BFS) and depth-first search (DFS), which explores both local-neighborhood linkage and correlation with distant nodes simultaneously. To reflect the locality around each node, a random walk with restarting mechanism (called random surfing) is applied in learning point-wise mutual information (PMI) representations (Cao et al., 2016). For capturing multi-scale representations of different-order neighborhoods, hierarchical random walks by skipping some of the nodes on paths are also proposed (Perozzi et al., 2017; Chen et al., 2018). Recently, Schlotterer et al. (Schlötterer et al., 2019) observed that RW-based methods perform better than others in exploring a wide range of distance and evaluated these methods as being helpful for SP distance estimation. However, a specific and insightful investigation of RW-based SP representation remains to be studied. In this paper, we discuss a novel biased random walk strategy toward high-order SP exploration and provide an explicit optimization algorithm for distance-preserved representation.

A.2 Efficient Implementation of BCDR Algorithm

We discuss here an efficient implementation to integrate the techniques mentioned in Section 3.1 and 3.2. Our algorithm is presented in Algorithm 1, including constructing SP representations and answering online distance queries. The description and analysis of these procedures are provided as follows.

Algorithm 1: construct SP representations & answer distance queries

Input: input graph $G = (V, E)$, set of landmarks L, distance queries of node pairs Q, dimension of embeddings d, number of walk paths on each node w_{in}, length of walk paths l_{in}, BC decay coefficient ζ, number of resampled walk paths on each node w_{out}, length of resampled walk paths l_{out}, distance decay coefficient α, training epochs m, learning rate η_r, usage of fast query τ.

Output: SP representation Z, distance predictor g_ϕ, queried distance D.

1 **Def** `sim_DT_with_BC` (G, L) **:**
2 distance triplets $T :=$ list$\{\}$, approximate BCs $\gamma :=$ dict$\{v_i : 0, \forall v_i \in V\}$
3 **for** *each landmark* $v_i \in L$ **do**
4 $\gamma[l_i] \leftarrow 1$
5 **for** *each node* $v_j \in V$ *reached by BFS from* v_i **do**
6 append (v_i, v_j, D_{ij}) to T
7 $\gamma[v_j] \leftarrow \gamma[v_j] + \frac{1}{D_{ij}}$
8 **end**
9 **end**
10 **return** T, γ
11 **Def** `sim_BC_Walk` (G, v_i, w_{in}, l_{in}, γ) **:**
12 distance map $D_i :=$ dict$\{v_i : 0\}$, visit counter $B :=$ dict$\{v_j : 0, \forall v_j \in V\}$
13 **for** *walk* k *from* 0 *to* w_{in} **do**
14 visit sign set $S_i := \{v_i\}$, current node $v_c := v_i$, length $c_i := 0$
15 **while** $c_i < l_{in}$ **do**
16 probabilities of the next candidate nodes $\tilde{P}_c^k :=$ dict$\{\}$
17 **for** $v_j \in \mathcal{N}_c \wedge v_j \notin S_i$ **do**
18 $\tilde{P}_c^k[v_j] \leftarrow \gamma[v_i] \times (2 - \tanh(\zeta - B[v_j]))$
19 **if** $v_j \in D_i$ **then**
20 $D_i[v_j] = \min\{D_i[v_j], D_i[v_c] + 1\}$
21 **else**
22 $D_i[v_n] = D_i[v_c] + 1$
23 **end**
24 **end**
25 sample next v_n from normalized $\tilde{P}_c^k$
26 $v_c \leftarrow v_n,\ S_i \leftarrow v_n, c_i \leftarrow c_i + 1,$ $B[v_n] \leftarrow B[v_n] + 1$
27 **end**
28 **end**
29 **return** D_i
30 **Def** `cons_BCDR` (G, d, L, w_{in}, l_{in}, ζ, w_{out}, l_{out}, α, m, η) **:**
31 $T, \gamma \leftarrow$ `sim_DT_with_BC` (G, L)
32 observed paths $P =$ list$\{\}$
33 **for** $v_i \in V$ **do**
34 $D_i \leftarrow$ `sim_BC_Walk` (G, v_i, w_{in}, l_{in}, γ)
35 probabilities of candidates nodes $\tilde{P}_i =$ dict$\{\}$
36 **for** $v_j \in D_i.keys$ **do**
37 $\tilde{P}_i[v_j] := \alpha^{D_i[v_j]} \cdot \gamma[v_j]$
38 **end**
39 **for** *walk* k *from* 0 *to* w_{out} **do**
40 sample walk path p_i of length l_{out} by normalized $\tilde{P}_i$
41 append p_i to P
42 **end**
43 **end**
44 maximize Equation 6 with $Z_{N\times d}$ and P by skip-gram algorithm.
45 define learnable distance predictor $g_\phi := (\mathbb{R}^d, \mathbb{R}^d) \rightarrow \mathbb{R}$
46 **for** *each epoch from* 0 *to* m **do**
47 $L_{MSE}(v_a, v_b) := [g_\phi(\mathbf{Z}_a, \mathbf{Z}_b) - D_{ab}]^2,\ \forall (v_a, v_b, D_{ab}) \in T$
48 minimize loss L_{MSE} with ϕ at the learning rate η_r by SGD.
49 **end**
50 **return** Z, g_ϕ
51 **Def** `query_BCDR` (Q, Z, g_ϕ, τ [, E]) **:**
52 estimated distance $D[v_a, v_b] = g_\phi(\mathbf{Z}_a, \mathbf{Z}_b),\ \forall (v_a, v_b) \in Q$
53 **if** not τ **then**
54 $D[v_a, v_b] \leftarrow 1,\ \forall (v_a, v_b) \in Q \cap E$
55 **end**
56 **return** D

A.2.1 SIMULATION OF DISTANCE TRIPLETS & BC WALK

To simulate distance triplets (line 1 to 10), we perform BFS from a fixed number of landmarks L and record their distance to each node on the graph (line 5 and 6). L comprises nodes that are selected by heuristic strategies (e.g., by their degrees in descending order or randomly), and the simulated triplets with linear complexity reflect a sufficient group of distance relations among $V \times V$ for metric learning. Before simulating BC-based walks, pre-computed BC of each node is also required at first, which takes at least $O(NM)$ time on unweighted graphs for exact solution. To reduce the time complexity, we consider a time-efficient approximation by integrating this process into the above simulation of distance triplets (line 7). Intuitively, $BC(v_a)$ measures some kind of relationship between v_a and the centers of the graph, and nodes with larger BC value possess a shorter average SP distance to any node on the graph. Since BFS visits each node just in ascending order of distance, we thus estimate BC on each node by the average distance to all landmarks in L without introducing extra time complexity.

Then, in the simulation of BC-based walks (line 11 to 29), we are interested in nodes that are covered by BC-based walks instead of the walk paths themselves, and the former with their distance to the root v_i (i.e., D_i) will be passed to feed subsequent construction (line 34). Therefore, we enlarge the node coverage by a decay mechanism on BC to diverge different walks. Note that BC-based walk possessing the ability to explore distant nodes tends to choose the paths that are probable to travel further, which causes ignorance of nodes on some dead ends. Addressing this, as stated in line 18, the probability of transiting to a node with large BC will be saturated after a sufficient number of walks passing through it, which means some rare paths are getting much easier to be visited later.

A.2.2 LEARNING EMBEDDINGS & DISTANCE PREDICTOR

To learn node embeddings Z on SP structures (line 31 to 44), we initially sample a group of BC-based walk paths as distance maps $\{D_i\}$ (line 34), and then resample from them to feed the skip-gram algorithm by considering distance decay and BC (line 37 and line 40), which preserves the property of distance relations discussed in Theorem 1. Besides, the resampling process also provides a shape transform of observed node sequences from $w_{in} \times l_{in}$ to $w_{out} \times l_{out}$. Let $\beta = (w_{in} l_{in})/(w_{out} l_{out}) > 1$, and this property leads the actual time cost of learning embeddings to be reduced to its $1/\beta$, in terms of learning directly on the original BC-based walks.

For the learning of the distance predictor (line 31, and line 45 to 49), we utilize a two-layer fully connected neural network as the predictor, which takes the concatenation of two nodes' embeddings as input, and outputs a scalar to indicate the distance (line 45). The predictor model is learned from distance triplets T by minimizing a mean squared error (MSE) between the predicted value and the real distance using the stochastic gradient descent (SGD) technique. Finally, the parameter of neural network ϕ and node embeddings Z are stored as graph SP representations.

A.2.3 ANSWERING DISTANCE QUERIES

For distance queries, We provide two versions with different properties based on the same SP representations. As revealed in previous studies of learning-based SP representation methods, the distance relations in local neighborhoods are really hard to converge, which causes a decline in average accuracy (Rizi et al., 2018; Kutuzov et al., 2019). For an input query pair (v_a, v_b), it is helpful to alleviate such decline if we perform an extra search among first-order neighbors (i.e., search in the adjacency matrix) to judge if (v_a, v_b) is an edge in the graph. Since this practice prolongs the total response time, we also preserve a fast version (BCDR-FQ) without neighbors searching for some potential applications.

A.2.4 PARALLELISM

The implementation of BCDR is easy to be highly-parallelized. In detail, the construction of SP representations could be divided into three parts, including simulating distance triplets, performing BC-based walks, training embeddings, as well as the distance predictor. First, the BFS from each landmark could be parallelized at a thread level up to the size of the landmark set. Second, for the simulation of BC-based walks, walks from different roots could also be simulated simultaneously. Third, the training process in the skip-gram algorithm and neural network could be locally parallelized by matrix computations.

A.3 THEOREM FOR CLARIFYING THE SIGNIFICANCE OF BC-BASED RANDOM WALK

Theorem 2. *Define $\mathcal{N}_a^{(h)} = \{v_j | D_{aj} = h\}$ as a set of nodes that are h-hops away from v_a and $N_h(v_a) = |\mathcal{N}_a^{(h)}|$ as the number of nodes in the set. Nodes in $\mathcal{N}_a^{(h)}$ could be divided into two sets, i.e., $e_h(v_a)$ and $f_h(v_a)$. Thereinto, $e_h(v_a)$ comprises nodes that have an edge with the nodes in $\mathcal{N}_a^{(h+1)}$ (called connective nodes), and $f_h(v_a)$ comprises the other nodes (called final nodes). The BC value of each node is approximated by considering only the shortest path of nodes within a range of k-hops locally. Let $\tilde{P}_R(\mathcal{N}_h(v_a) \to \mathcal{N}_{h+1}(v_a))$ represent the probability to transit from $\mathcal{N}_h(v_a)$ to $\mathcal{N}_{h+1}(v_a)$ by a naive random walk, and $\tilde{P}_B(\mathcal{N}_h(v_a) \to \mathcal{N}_{h+1}(v_a))$ represent that by a BC-based random walk. Let $\tilde{P}_R(f_h(v_a) \to e_h(v_a))$ be the probability of transition from $f_h(v_a)$ to $e_h(v_a)$. $\mathcal{E}(v_a)$ is the eccentricity of v_a, $\mathcal{E}(v_a) = \max_{v_b \in G} D_{ab}$. Then, for sufficient large $\mathcal{E}(v_a)$, any node $v_a \in G$ and any $h > 1$,*

$$\frac{\tilde{P}_B(\mathcal{N}_h(v_a) \to \mathcal{N}_{h+1}(v_a))}{\tilde{P}_R(\mathcal{N}_h(v_a) \to \mathcal{N}_{h+1}(v_a))} = 1 + B(k) + C \tag{12}$$

$$\begin{aligned} &\lim_{k \to \mathcal{E}(v_a)-1-h} B(k) + C = \frac{A_2 - 1}{A_1} + C > 0 \\ &A_1 = \frac{|e_h(v_a)|}{|f_h(v_a)|}, \quad A_2 = \frac{1}{\tilde{P}_R(f_h(v_a) \to e_h(v_a))}, \quad C \geq 0. \end{aligned} \tag{13}$$

Proof. We simplify symbols $\mathcal{N}_h(v_a), N_h(v_a), e_h(v_a), f_h(v_a)$ as $\mathcal{N}_h, N_h, e_h, f_h$ for short.

$$\begin{aligned}\overrightarrow{N}_h &= \#(\bigcup_{i=h}^{\min\{\mathcal{E}(v_a),h+k-1\}} \{v_j | v_j \in \mathcal{N}_a^{(i)}\}) \\ \overleftarrow{N}_h &= \#(\bigcup_{i=\max\{0,h-k+1\}}^{h} \{v_j | v_j \in \mathcal{N}_a^{(i)}\})\end{aligned} \tag{14}$$

where $\#(\cdot)$ is a counting function indicating the number of occurrence times of specified nodes, i.e., the cardinality of a sampled set.

According to the definition in Theorem 2, we have $N_h = |e_h| + |f_h|$. Since only nodes in e_h could travel from $\mathcal{N}_h$ to $\mathcal{N}_{h+1}$, We firstly consider $\tilde{P}_R(e_h \to e_{h+1} | e_h \to \mathcal{N}_{h+1})$ and $\tilde{P}_B(e_h \to e_{h+1} | e_h \to \mathcal{N}_{h+1})$.

For general random walks, the choice of destination is based on uniform sampling, thus causing

$$\tilde{P}_R(e_h \to e_{h+1} | e_h \to \mathcal{N}_{h+1}) = \frac{|e_{h+1}|}{N_{h+1}} \tag{15}$$

For BC-based random walk, we need calculate BC value of nodes of e_{h+1} and f_{h+1} for starters. Let $\mathrm{BC}(e_{h+1})$ and $\mathrm{BC}(f_{h+1})$ represent the BC value of nodes in e_{h+1} and f_{h+1} respectively, and the correspond legal SPs counts come from 4 sources as $\{\overleftarrow{\mathcal{N}}_h \to \overrightarrow{\mathcal{N}}_{h+2}\}$, $\{\overleftarrow{\mathcal{N}}_h \to \mathcal{N}_{h+1}\}$, $\{\mathcal{N}_{h+1} \to \overrightarrow{\mathcal{N}}_{h+2}\}$ and $\{\mathcal{N}_{h+1} \to \mathcal{N}_{h+1}\}$. And we use $\mathrm{BC}(\{\cdot \to \cdot\})$ as the BC gain from the specified source, then

$$\begin{aligned}&\mathrm{BC}(\{\overleftarrow{\mathcal{N}}_h \to \overrightarrow{\mathcal{N}}_{h+2}\}) = \overleftarrow{N}_h \overrightarrow{N}_{h+2} \\ &\mathrm{BC}(\{\overleftarrow{\mathcal{N}}_h \to \mathcal{N}_{h+1}\}) = \overleftarrow{N}_h (|f_{h+1}| \cdot 0 + |e_{h+1}| \beta_e^{(1)}) \\ &\mathrm{BC}(\{\mathcal{N}_{h+1} \to \overrightarrow{\mathcal{N}}_{h+2}\}) = \overrightarrow{N}_{h+2} (|f_{h+1}| \cdot 1 + |e_{h+1}| \beta_e^{(1)}) \\ &\mathrm{BC}(\{\mathcal{N}_{h+1} \to \mathcal{N}_{h+1}\}) = N_{h+1}^2 \beta_e^{(2)}\end{aligned} \tag{16}$$

where $\beta_e^{(1)}$ means average BC gain between nodes in e_{h+1} and $\overrightarrow{\mathcal{N}}_{h+2}$, and $\beta_e^{(2)}$ means average BC gain between nodes both in e_{h+1}, which are constantly related with G. Therefore, we have

$$\mathrm{BC}(e_{h+1}) = \overleftarrow{N}_h \overrightarrow{N}_{h+2} + (\overleftarrow{N}_h + \overrightarrow{N}_{h+2}) |e_{h+1}| \beta_e^{(1)} + \overrightarrow{N}_{h+2} |f_{h+1}| + N_{h+1}^2 \beta_e^{(2)} \tag{17}$$

Likewise, we calculate

$$\begin{aligned}\mathrm{BC}(f_{h+1}) =& \overleftarrow{N}_h \overrightarrow{N}_{h+2} \cdot 0 + \overleftarrow{N}_h (|f_{h+1}| \beta_f^{(1)} + |e_{h+1}| \cdot 0) + \overrightarrow{N}_{h+2} (|f_{h+1}| \beta_f^{(1)} + e_{h+1} \cdot 0) + N_{h+1}^2 \beta_e^{(2)} \\ =& (\overleftarrow{N}_h + \overrightarrow{N}_{h+2}) \beta_f^{(1)} + N_{h+1}^2 \beta_f^{(2)}\end{aligned} \tag{18}$$

To compare the above $\mathrm{BC}(e_{h+1})$ and $\mathrm{BC}(f_{h+1})$,

$$\frac{\mathrm{BC}(f_{h+1})}{\mathrm{BC}(e_{h+1})} = \frac{(\overleftarrow{N}_h + \overrightarrow{N}_{h+2}) \beta_f^{(1)} + N_{h+1}^2 \beta_f^{(2)}}{\overleftarrow{N}_h \overrightarrow{N}_{h+2} + (\overleftarrow{N}_h + \overrightarrow{N}_{h+2}) |e_{h+1}| \beta_e^{(1)} + \overrightarrow{N}_{h+2} |f_{h+1}| + N_{h+1}^2 \beta_e^{(2)}} \tag{19}$$

note that for any N_j and $N_{(x,y)} = \overrightarrow{N}_0 - \overleftarrow{N}_x - \overrightarrow{N}_y$ where $j, x, y \in \{0, \mathcal{E}(v_a)\}$,

$$\lim_{k \to \mathcal{E}(v_a)-1-h} \frac{N_j}{N_{(x,y)}} = \lim_{k \to \mathcal{E}(v_a)-1-h} \epsilon(k) = 0 \tag{20}$$

Equation 18 is reduced to

$$\frac{\mathrm{BC}(f_{h+1})}{\mathrm{BC}(e_{h+1})} = \frac{2\epsilon(k)\beta_f^{(1)} + \epsilon(k^2)\beta_f^{(2)}}{1 + 2\epsilon(k) n |e_{h+1}| \beta_e^{(1)} + \epsilon(k) |f_{h+1}| + \epsilon(k^2) \beta_e^{(2)}} = 2\beta_f^{(1)} \epsilon(k) \tag{21}$$

Then, we perform weighted random sampling based on BC and get

$$\tilde{P}_B(e_h \to e_{h+1} | e_h \to \mathcal{N}_{h+1}) = \frac{|e_{h+1}|}{|e_{h+1}| + 2|f_{h+1}| \beta_f^{(1)} \epsilon(k)} \tag{22}$$

Now, we consider the relation between $\tilde{P}_R(\mathcal{N}_h \to e_{h+1}|\mathcal{N}_h \to \mathcal{N}_{h+1})$ and $\tilde{P}_B(\mathcal{N}_h \to e_{h+1}|\mathcal{N}_h \to \mathcal{N}_{h+1})$.

$$\begin{aligned}
\frac{\tilde{P}_B(\mathcal{N}_h \to \mathcal{N}_{h+1})}{\tilde{P}_R(\mathcal{N}_h \to \mathcal{N}_{h+1})} &= \frac{\tilde{P}_B(e_h)\tilde{P}_B(e_h \to \mathcal{N}_{h+1})}{\tilde{P}_R(e_h)\tilde{P}_R(e_h \to \mathcal{N}_{h+1})} \\
&= \frac{\tilde{P}_B(\mathcal{N}_{h-1} \to e_h) + \tilde{P}_B(\mathcal{N}_{h-1} \to f_h)\tilde{P}_B(f_h \to e_h)}{\tilde{P}_R(\mathcal{N}_{h-1} \to e_h) + \tilde{P}_R(\mathcal{N}_{h-1} \to f_h)\tilde{P}_R(f_h \to e_h)} \\
&= 1 + \frac{\left[\tilde{P}_B(\mathcal{N}_{h-1} \to e_h) - \tilde{P}_R(\mathcal{N}_{h-1} \to e_h)\right][1 - \tilde{P}_R(f_h \to e_h)]}{\tilde{P}_R(\mathcal{N}_{h-1} \to e_h) + \tilde{P}_R(\mathcal{N}_{h-1} \to f_h)\tilde{P}_R(f_h \to e_h)} \\
&\quad + \frac{\tilde{P}_R(f_h \to e_h)\epsilon}{\tilde{P}_R(\mathcal{N}_{h-1} \to e_h) + \tilde{P}_R(\mathcal{N}_{h-1} \to f_h)\tilde{P}_R(f_h \to e_h)} \\
&= 1 + \frac{|f_h|[1 - 2|f_h|\beta_f^{(1)}\epsilon(k)][1 - \tilde{P}_R(f_h \to e_h)]}{(1 + \frac{|f_h|}{|e_h|})[|e_h| + 2|f_h|\beta_f^{(1)}\epsilon(k)]\tilde{P}_R(f_h \to e_h)} \\
&\quad + \frac{\tilde{P}_R(f_h \to e_h)\epsilon}{\tilde{P}_R(\mathcal{N}_{h-1} \to e_h) + \tilde{P}_R(\mathcal{N}_{h-1} \to f_h)\tilde{P}_R(f_h \to e_h)}
\end{aligned} \tag{23}$$

Let $C = \frac{\tilde{P}_R(f_h \to e_h)\epsilon}{\tilde{P}_R(\mathcal{N}_{h-1} \to e_h) + \tilde{P}_R(\mathcal{N}_{h-1} \to f_h)\tilde{P}_R(f_h \to e_h)}$, $B(k) = \frac{|f_h|[1 - 2|f_h|\beta_f^{(1)}\epsilon(k)][1 - \tilde{P}_R(f_h \to e_h)]}{(1 + \frac{|f_h|}{|e_h|})[|e_h| + 2|f_h|\beta_f^{(1)}\epsilon(k)]\tilde{P}_R(f_h \to e_h)}$. Since C is a non-negative value independent of k, finally we get

$$\frac{\tilde{P}_B(\mathcal{N}_h \to \mathcal{N}_{h+1})}{\tilde{P}_R(\mathcal{N}_h \to \mathcal{N}_{h+1})} = 1 + B(k) + C \tag{24}$$

where

$$\lim_{k \to \mathcal{E}(v_a) - 1 - h} B(k) + C = \frac{A_2 - 1}{A_1} + C. \tag{25}$$

□

Remark 1. *Equation 12 and 13 in Theorem 2 give definite conditions under which BC-based walk travels further than random walk. Since nodes in v_a's h-order neighborhood $\mathcal{N}_a^{(h)}$ could be always divided into $e_h(v_a)$ and $f_h(v_a)$ like Figure 3a, BC-based walk improves exploration distance beyond local loops and dead ends in contrast with naive random walk by two aspects. On one side, even if $\mathcal{N}_a^{(h)}$ comprises a larger number of nodes in $f_h(v_a)$ than $e_h(v_a)$ and thus A_1 decreases, BC-based walk will tends to transit in $e_h(v_a)$ to get near with the next desired set $\mathcal{N}_a^{(h+1)}$. On the other side, even if nodes in $f_h(v_a)$ have fewer links to those in $e_h(v_a)$ and thus A_2 increases, BC-based walk tends to transit between $f_h(v_a)$ and $e_h(v_a)$ instead of looping within $f_h(v_a)$ as well as $\mathcal{N}_a^{(h-1)}$.*

A.4 Proof of Proposition 1

Proof. In Proposition 1, we optimize an approximate objective $\hat{\mathcal{L}}_n$ instead of $\mathcal{L}_n$, i.e.,

$$\hat{\mathcal{L}}_n(Z) = \sum_{v_i \in V} \tilde{P}(v_i)\left\{\mathbb{E}_{v_j \sim \tilde{Q}_{W_i}(V)}[\log \sigma(\mathbf{Z}_i\mathbf{Z}_j^T)] + \lambda \mathbb{E}_{v_k \sim \tilde{P}_n(V)}[\log \sigma(-\mathbf{Z}_i\mathbf{Z}_k^T)]\right\} \tag{26}$$

Here, we rewrite the negative sampling item of Equation 26 as

$$\begin{aligned}
\mathbb{E}_{v_k \sim \tilde{P}_n(W_i)}[\log \sigma(-\mathbf{Z}_i\mathbf{Z}_k^T)]) &= \sum_{v_k \in W_i} \tilde{P}_n(v_k|v_i)[\log \sigma(-\mathbf{Z}_i\mathbf{Z}_k^T)] \\
&= \tilde{P}_n(v_j|v_i)[\log \sigma(-\mathbf{Z}_i\mathbf{Z}_j^T)] + \sum_{v_k \in W_i \setminus \{v_j\}} \tilde{P}_n(v_k|v_i)[\log \sigma(-\mathbf{Z}_i\mathbf{Z}_k^T)]
\end{aligned} \tag{27}$$

Then, for each pair of $v_i \in V$ and $v_j \in W_i$, we get independent objective by combing similar items from the total likelihood $\hat{\mathcal{L}}_n$, and reach

$$\begin{aligned}
\hat{\mathcal{L}}_n(Z) &= \sum_{v_i \in V} \sum_{v_j \in W_i} \mathcal{L}'(\mathbf{Z}_i, \mathbf{Z}_j) \\
\mathcal{L}'(\mathbf{Z}_i, \mathbf{Z}_j) &= \tilde{P}(v_i, v_j) \log \sigma(-\mathbf{Z}_i\mathbf{Z}_j^T) + \lambda \tilde{P}(v_i)\tilde{P}_n(v_j|v_i) \log \sigma(-\mathbf{Z}_i\mathbf{Z}_j^T)
\end{aligned} \tag{28}$$

Let $\hat{D} = ZZ^T$, for each node pair (v_a, v_b) with SP distance $\hat{D}_{ab}$, consider

$$\hat{D}_{ab} = \mathbf{Z}_a \mathbf{Z}_b^T = \arg\max_{\mathbf{Z}_a, \mathbf{Z}_b} \mathcal{L}'(\mathbf{Z}_a, \mathbf{Z}_b) \tag{29}$$

Remember that $\tilde{Q}_{W_i}$ is a distribution resampled from $\tilde{P}_{W_i}$, as an efficient approximation to $\tilde{P}_{\mathring{W}_i}$, i.e.,

$$\tilde{Q}_{W_i}(v_j) = \frac{\alpha^{D_{ij}} \mathrm{BC}(v_j)}{\sum_{v_k \in W_i} \alpha^{D_{ik}} \mathrm{BC}(v_k)} \tag{30}$$

Denote $BC(v_b)$ by γ_b, according to Equation 30, the joint distribution of each pair (v_a, v_b) could be formulated as

$$\tilde{P}(v_a, v_b) = \tilde{P}(v_a) \cdot \tilde{P}(v_b|v_a) = \tilde{P}(v_a) \cdot \alpha^{D_{ab}} \gamma_b \tag{31}$$

Then, consider the formualtion of $\tilde{P}_n(v_b|v_a)$. Recall that the negative sampling is a uniform distribution on W_a which are simulated by BC-based walk, and the probability of v_b's occurrence relies on γ_b and $\mathcal{W}_a$. Thus there holds

$$\tilde{P}_n(v_b|v_a) = \frac{\gamma_b}{\kappa(v_a)} \tag{32}$$

where $\kappa(v_a)$ is in proportion with the number of nodes covered by $\mathcal{W}_a$ on the graph.

Furthermore, Equation 29 could be rewritten as

$$\hat{D}_{ab} = \arg\max_{\hat{D}_{ab}} \tilde{P}(v_a) \alpha^{D_{ab}} \gamma_b \log \sigma(\hat{D}_{ab}) + \frac{\lambda}{\kappa(v_a)} \tilde{P}(v_a) \gamma_b \log \sigma(-\hat{D}_{ab}) \tag{33}$$

Solve the above problem by just let $\frac{\partial \mathcal{L}(v_a, v_b)}{\partial \hat{D}_{ab}}$ be equal to zero, i.e.,

$$\frac{\partial \mathcal{L}(v_a, v_b)}{\partial \hat{D}_{ab}} = \quad \tilde{P}(v_a) \alpha^n \gamma_b \sigma(1 - \hat{D}_{ab}) - \frac{\lambda}{\kappa(v_a)} p(v_a) \gamma_b \sigma(1 + \hat{D}_{ab}) = 0 \tag{34}$$

After some simplification, we get

$$\hat{D}_{ab} = D_{ab} \log \alpha - \log \frac{\lambda}{\kappa(v_a)} \tag{35}$$

Let $\epsilon = \lambda \kappa^{-1}(v_a)$ and there holds

$$\hat{D}_{ab} = -\log \epsilon + D_{ab} \log \alpha \tag{36}$$

□

A.5 Remark for the Relationship between Distance Matrix & Distance-based Similarity Matrix

Remark 2. *Equation 7 in Proposition 1 reveals the linear projections between elements in $\hat{D}$ and D. Thereinto, $-\log \epsilon$ is a big positive constant with respect to $|log|W_a|| - |\log \lambda|$, and $D_{ab} \log \alpha$ is a negative value that decreases linearly with SP distance D_{ab}. It indicates that there exists a finite distance range $n \in \mathbb{N}_+$, for each node $v_b \in \{v_x | D_{ax} \leq n\}$, the distance relation between v_a and v_b could be well-optimized by converging $Z_a Z_b^T \to \hat{D}_{ab} > 0$. It also reveals that the significance of* distance resampling *is to preserve the SP distance relations between nodes which are well-observed on given arbitrary walk paths. Besides, although the similarity matrix $\hat{D}$ could not directly tell the absolute distance, it also shares similar properties with D, i.e., if we fix v_a as the source node in a path, the comparison between the similarities of (v_a, v_b) and (v_a, v_c) just reflects the SP distance relations between them. This practical property is discussed in Theorem 1.*

A.6 Proof of Theorem 2

Proof. In terms of node pair (v_a, v_b), as proved in Proposition 1, their similarity $\hat{D}_{ab}$ in the embedding space varies linear with respect to the SP distance D_{ab} on the graph, i.e.,

$$\hat{D}_{ab} = -\log \epsilon + D_{ab} \log \alpha \tag{37}$$

Likewise, for (v_a, v_c), there holds

$$|\hat{D}_{ac}| = -\log \epsilon + D_{ac} \log \alpha \tag{38}$$

where $0 < \alpha < 1$ and ϵ relies on W_a which is independent of v_b and v_c.

Then, consider the distance relation of v_a, v_b and v_c, there holds

$$(D_{ab} - D_{ac})(\hat{D}_{ab} - \hat{D}_{bc}) = (D_{ab} - D_{ac})((D_{ab} - D_{ac})) \log \alpha = \log \alpha \cdot (D_{ab} - D_{ac})^2 \leq 0. \tag{39}$$

□

A.7 DATASETS

To thoroughly evaluate our proposed method, we conduct experiments on real-world graphs and synthetic graphs with divergent properties on sizes, structures, diameters, etc. Thereinto, real-world graphs are extracted from Stanford Large Network Dataset Collection (Leskovec & Krevl, 2014), and synthetic graphs are simulated according to specific rules described in A.7.6. The visualization results of each graph are illustrated in Figure 6, and the corresponding statistics are presented in Table 3. In the experiments, we show the efficiency and scalability of BCDR on real-world graphs of different sizes and test on smaller synthetic graphs with different structures for further analysis of exploration range and distance preservation. Here are brief descriptions of these graphs:

A.7.1 CORA

This is a graph that describes the citation relationship of papers, which contains 2708 nodes and 10556 directed edges among them. Each node also has a predefined feature with 1433 dimensions.

A.7.2 FACEBOOK

This is a graph that describes the relationship among Facebook users by their social circles (or friend lists), which is collected from a group of test users. Facebook has also encoded each user with a reindexed user ID to protect their privacy.

A.7.3 GRQC

This is a graph recorded from the e-print arXiv in the period from January 1993 to April 2003, which represents co-author relationships based on their submission. Each undirected edge (v_i, v_j) represents that an author v_i is co-authored a paper with another author v_j. If one paper is owned by k authors, a complete subgraph of k nodes is generated correspondingly.

A.7.4 DBLP

This is a graph collected as a computer science bibliography that provides a comprehensive list of research papers in computer science. As an undirected collaboration network, each edge reflects the corresponding two authors who have at least one paper together.

A.7.5 YOUTUBE

This is a graph constructed from users' social relations on a video-sharing website Youtube. Each node represents a user, and each edge indicates a friendship between two users.

A.7.6 SYNTHETIC GRAPHS

We also some smaller graphs reflecting one or some of the typical sub-structures which are frequently occurred in complex graphs. The simulation rules of each graph are listed as follows.

- Circle Graph (CG): this is a graph that contains several circles of different sizes. The simulation of circle graphs takes an iterative process where for each newly introduced circle, there are a limited number of nodes (called exit nodes) connected to the previous circles.

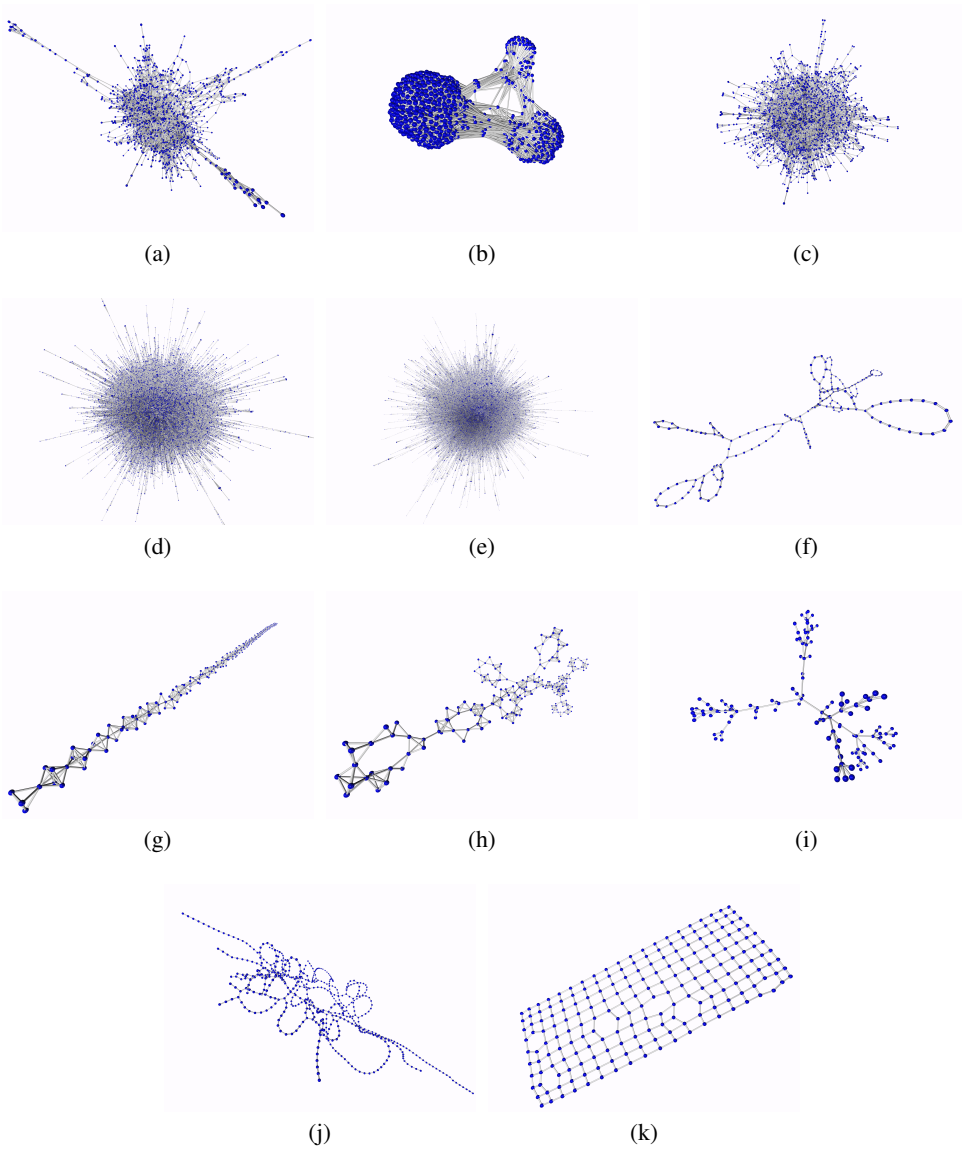

Figure 6: Visualization results of the graphs used for evaluation. **(a):** Cora. **(b):** Facebook. **(c):** GrQc. **(d):** DBLP. **(e):** YouTube. **(f):** CG. **(g):** TG. **(h):** TCG. **(i):** TRG. **(j):** SG. **(k):** NG.

- Triangle Graph (TG): this is a graph possessing several cliques which are linearly connected mutually.
- Tri-circle Graph (TCG): this is a graph that combines the properties of circle graphs and triangle graphs. Here, each circle is simulated by connecting triangle sub-graphs end to end.
- Tree Graph (TRG): this is a graph that is generated from one root to several leaves recursively. There is no cycle in tree graphs. To control the tree structure, we define a splitting probability that is decayed exponentially with current depth.
- Spiral Graph (SG): this is a graph shaped like a spiral line. We first simulate a line graph and add edges between nodes with exponentially increased distances by their indices on the line.
- Net Graph (NG): this is a graph containing grid-like connections between nodes. We define a small probability of dropping those edges stochastically.

Table 3: Statistics of the graphs used for evaluation. N denotes the number of nodes, M denotes the number of edges, RoBC denotes the range of BC, mBC denotes the average BC on nodes, $\mathcal{D}$ denotes the diameter of a graph, BFS denotes the average processing time of breadth-first search on all nodes. Each graph is considered an undirected and unweighted graph in the SP representation problem.

	N	M	M/N	$\mathcal{D}$	RoBC	mBC	BFS
Cora	$2,708$	$10,787$	3.9834	21	375.20	2.7174	0.0074 s
Facebook	$4,039$	$176,437$	21.846	8	$1,306.9$	0.8993	0.0191 s
GrQc	$5,242$	$30,042$	5.7310	17	148.43	2.7219	0.0148 s
DBLP	$317,080$	$1,049,866$	3.3110	21	$1,140.9$	2.0795	46.0907 s
YouTube	$1,134,890$	$5,975,248$	5.2650	20	-	-	691.0986 s
CG	197	216	1.0964	46	0.6058	0.1032	-
TG	384	984	2.5625	100	0.4987	0.0928	-
TCG	242	594	2.4545	31	0.4891	0.0551	-
TRG	134	133	0.9925	12	0.6416	0.0630	-
SG	550	585	1.0636	85	0.3068	0.0528	-
NG	200	364	1.8200	28	0.2914	0.1215	-

A.8 Extended Results on Performance of SP Distance Query

We present in Table 4 and 5 the full experimental results of comparisons to approximate SP representation methods and GRL methods. For the former, the configuration is the same as described in the main paper. For the latter, only the approximation quality (i.e., mAE and mRE) is evaluated, and the metrics are exerted directly on the representations without quantizing the outputs to integers or checking adjacency matrices. We see from Table 5 that although general embeddings by GRL methods could preserve some local SP structures, our proposed method with explicit SP constraint possesses better approximation quality for the SP distance querying task.

A.9 Extended Results on Exploration Range of Distance

The extended results on all synthetic graphs are shown in Figure 7. We analyze the significance of utilizing BC-RW for wider range exploration on different structures as follows.

- For CGs and TCGs, BC-RW tends to choose the exit nodes of each circle since they provide a large BC gain by splitting all SPs between inner nodes and outer nodes regarding the current circle.
- For TGs, transitions on every triangle clique tend to move forward along the trunk road since the number of nodes beyond the current clique is often larger than that of inner nodes, contributing to more SPs.
- For TRGs, each transition from the root to leaves appears to be biased since subtrees with more descendants contribute to more SPs and possess larger BC values.
- For SGs, there are many shortcuts that link some nodes on the trunk road, and the BC values of shortcut nodes and other nodes are usually on par. BC-RW possesses a slight advantage by keeping a relatively good balance on these nodes.
- For NGs, most of the nodes are passed through by SPs with similar probabilities, and BC-RW is hard to tell the proper direction for deeper exploration like other walk strategies.

A.10 Extended Results on Preservation of Distance Relations

The extended results of distance preservation are shown in Figure 8 and 9. These figures confirm that our model is much more satisfactory in preserving distance relation than existing methods except for TGs. For most graphs, BC walk paths provide sufficient observation on each node by locating many distant nodes with a sequence of center nodes on a graph, and thus the resampling process based on such observation could preserve distance relations in the exploration range. For TGs,

Table 4: Full comparison of approximate methods on SP distance representations. PT denotes processing time when constructing SP representations, PMU denotes memory usage in such processing, SC denotes space cost on storing SP representations, RT denotes average response time of answering a distance query, QMU denotes memory usage in the querying stage, mAE and mRE are the metrics of accuracy loss. DNF means it did not finish in one day.

Dataset	Model	PT	PMU	SC	RT	QMU	mAE	mRE
Cora	ADO	**0.3179 s**	6.205 MB	0.9905 MB	9,813 ns	11.89 MB	2.1070	0.4266
	LS	**0.6355 s**	2.952 MB	0.6791 MB	11,537 ns	10.92 MB	1.0599	0.2068
	Orion	61.34 s	15.06 MB	**0.1655 MB**	**63.87 ns**	**0.1654 MB**	3.0542	0.5242
	Rigel	61.36 s	15.06 MB	**0.1655 MB**	**4,587 ns**	**0.2482 MB**	3.0464	0.5164
	DADL	68.22 s	27.36 MB	**0.1696 MB**	6,798 ns	0.2486 MB	1.0822	0.1862
	Path2Vec	172.9 s	2.870 MB	**0.1696 MB**	6,820 ns	0.2486 MB	3.2020	0.6066
	HALK	**30.44 s**	6.715 MB	**0.1696 MB**	6,802 ns	0.2486 MB	1.7702	0.3293
	BCDR (ours.)	40.58 s	**2.728 MB**	**0.1696 MB**	6,906 ns	0.2486 MB	**0.7008**	**0.1196**
	BCDR-FQ (ours.)	39.51 s	**2.728 MB**	**0.1696 MB**	**50.85 ns**	**0.1657 MB**	**0.7249**	**0.1247**
	BCDR-FC (ours.)	35.60 s	**2.728 MB**	**0.1696 MB**	6,830 ns	0.2486 MB	**0.8243**	**0.1384**
Facebook	ADO	**1.991 s**	13.10 MB	1.783 MB	8,105 ns	16.94 MB	1.1842	0.5080
	LS	**3.382 s**	**4.390 MB**	0.9929 MB	11,664 ns	12.28 MB	0.9566	0.3924
	Orion	80.53 s	21.00 MB	**0.2419 MB**	**60.81 ns**	**0.2418 MB**	1.7770	0.6864
	Rigel	80.31 s	21.00 MB	**0.2419 MB**	**4,976 ns**	**1.588 MB**	1.7531	0.6625
	DADL	176.3 s	42.44 MB	**0.2459 MB**	8,601 ns	**1.588 MB**	0.2250	0.0792
	Path2Vec	284.5 s	5.459 MB	**0.2459 MB**	8,582 ns	**1.588 MB**	1.4263	0.5489
	HALK	**75.95 s**	21.28 MB	**0.2459 MB**	8,777 ns	**1.588 MB**	0.9004	0.3517
	BCDR (ours.)	159.3 s	**5.213 MB**	**0.2459 MB**	8,705 ns	**1.588 MB**	**0.1086**	**0.0323**
	BCDR-FQ (ours.)	160.6 s	**5.213 MB**	**0.2459 MB**	**53.78 ns**	**0.2421 MB**	**0.0978**	**0.0385**
	BCDR-FC(ours.)	91.71 s	**5.213 MB**	**0.2459 MB**	8,713 ns	**1.588 MB**	**0.1463**	**0.0478**
GrQc	ADO	**1.322 s**	17.75 MB	2.922 MB	13,555 ns	19.19 MB	1.8747	0.3582
	LS	**2.098 s**	5.722 MB	1.315 MB	11,825 ns	13.60 MB	1.1538	0.2097
	Orion	98.14 s	21.33 MB	**0.3202 MB**	**62.80 ns**	**0.3201 MB**	3.0532	0.4849
	Rigel	98.00 s	21.33 MB	**0.3202 MB**	**4,872 ns**	**0.5519 MB**	3.0493	0.4810
	DADL	103.0 s	53.09 MB	**0.3242 MB**	6,912 ns	0.5523 MB	0.9812	0.1659
	Path2Vec	333.0 s	5.632 MB	**0.3242 MB**	6,938 ns	0.5523 MB	4.1239	0.7231
	HALK	**48.30 s**	13.80 MB	**0.3242 MB**	6,955 ns	0.5523 MB	1.1695	0.2063
	BCDR (ours.)	68.12 s	**5.351 MB**	**0.3242 MB**	7,003 ns	0.5523 MB	**0.7854**	**0.1316**
	BCDR-FQ (ours.)	67.98 s	**5.351 MB**	**0.3242 MB**	**51.90 ns**	**0.3204 MB**	**0.8743**	**0.1501**
	BCDR-FC (ours.)	58.30 s	**5.351 MB**	**0.3242 MB**	6,965 ns	0.5523 MB	**0.8776**	**0.1442**
DBLP	ADO	37,029 s	8,899 MB	199.8 MB	8,598 ns	5,980 MB	3.0691	0.4985
	LS	5,838 s	349.0 MB	80.02 MB	12,094 ns	344.6 MB	2.5060	0.3939
	Orion	5,531 s	321.8 MB	**19.36 MB**	**82.25 ns**	**19.35 MB**	3.5044	0.5165
	Rigel	5,523 s	321.8 MB	**19.36 MB**	**5,657 ns**	**35.37 MB**	3.5043	0.5164
	DADL	2,650 s	1,958 MB	**19.36 MB**	7,562 ns	**35.37 MB**	**1.2753**	0.2016
	Path2Vec	27,453 s	140.9 MB	**19.36 MB**	7,700 ns	**35.37 MB**	3.9474	0.6097
	HALK	1,270 s	649.6 MB	**19.36 MB**	7,704 ns	**35.37 MB**	1.8477	0.3077
	BCDR (ours.)	**1,086 s**	**53.52 MB**	**19.36 MB**	7,646 ns	**35.37 MB**	**1.1857**	**0.1712**
	BCDR-FQ (ours.)	**1,026 s**	**53.52 MB**	**19.36 MB**	**58.82 ns**	**19.35 MB**	1.3018	**0.1840**
	BCDR-FC (ours.)	**999.8 s**	**53.52 MB**	**19.36 MB**	7,617 ns	**35.37 MB**	**1.1014**	**0.1580**
Youtube	ADO	DNF	–	–	–	–	–	–
	LS	87,902 s	1,258 MB	286.7 MB	16,672 ns	1,217 MB	2.0159	0.4091
	Orion	50,484 s	1,251 MB	**69.26 MB**	**163.9 ns**	**69.26 MB**	2.8642	0.5473
	Rigel	51,246 s	1,251 MB	**69.26 MB**	13,808 ns	**114.9 MB**	2.8642	0.5473
	DADL	28,351 s	6,983 MB	**69.27 MB**	7,708 ns	**114.9 MB**	1.1144	0.2163
	Path2Vec	DNF	–	–	–	–	–	–
	HALK	**5,971** s	2,187 MB	**69.27 MB**	7,764 ns	**114.9 MB**	1.9035	0.3860
	BCDR (ours.)	**7,794 s**	**179.8 MB**	**69.27 MB**	7,585 ns	**114.9 MB**	**0.9080**	**0.1677**
	BCDR-FQ (ours.)	7,893 s	**179.8 MB**	**69.27 MB**	**63.78 ns**	**69.27 MB**	**0.9004**	**0.1704**
	BCDR-FC (ours.)	**6,000 s**	**179.8 MB**	**69.27 MB**	**6,156 ns**	**114.9 MB**	**0.9083**	**0.1745**

Table 5: Extended comparison to general GRL models on approximation quality

Model	Cora		Facebook		GrQc	
	mAE	mRE	mAE	mRE	mAE	mRE
LLE (Roweis & Saul, 2000)	5.6265	0.8445	1.9921	0.6841	4.8849	0.7105
LE (Roweis & Saul, 2000)	5.6393	0.8455	2.0312	0.6998	5.0046	0.7366
GF (Ahmed et al., 2013)	5.6249	0.8440	1.8743	0.6383	4.8562	0.7125
DeepWalk (Perozzi et al., 2014)	1.5183	0.2425	0.9323	0.3289	2.8002	0.4169
GraRep (Shaosheng et al., 2015)	2.6206	0.3830	2.8702	1.0479	4.2445	0.6292
Node2Vec (Grover & Leskovec, 2016)	1.3072	0.2115	0.8541	0.2993	1.5156	0.2278
NetMF (Qiu et al., 2018)	4.1736	0.6025	1.6982	0.6163	3.8799	0.5779
VERSE (Tsitsulin et al., 2018)	2.8895	0.4049	1.1092	0.3729	3.3436	0.4689
LPCA (Chanpuriya et al., 2020)	2.2813	0.3337	2.1373	0.8611	2.4526	0.3475
BCDR (ours.)	**0.9768**	**0.1605**	**0.4804**	**0.1770**	**1.0490**	**0.1684**

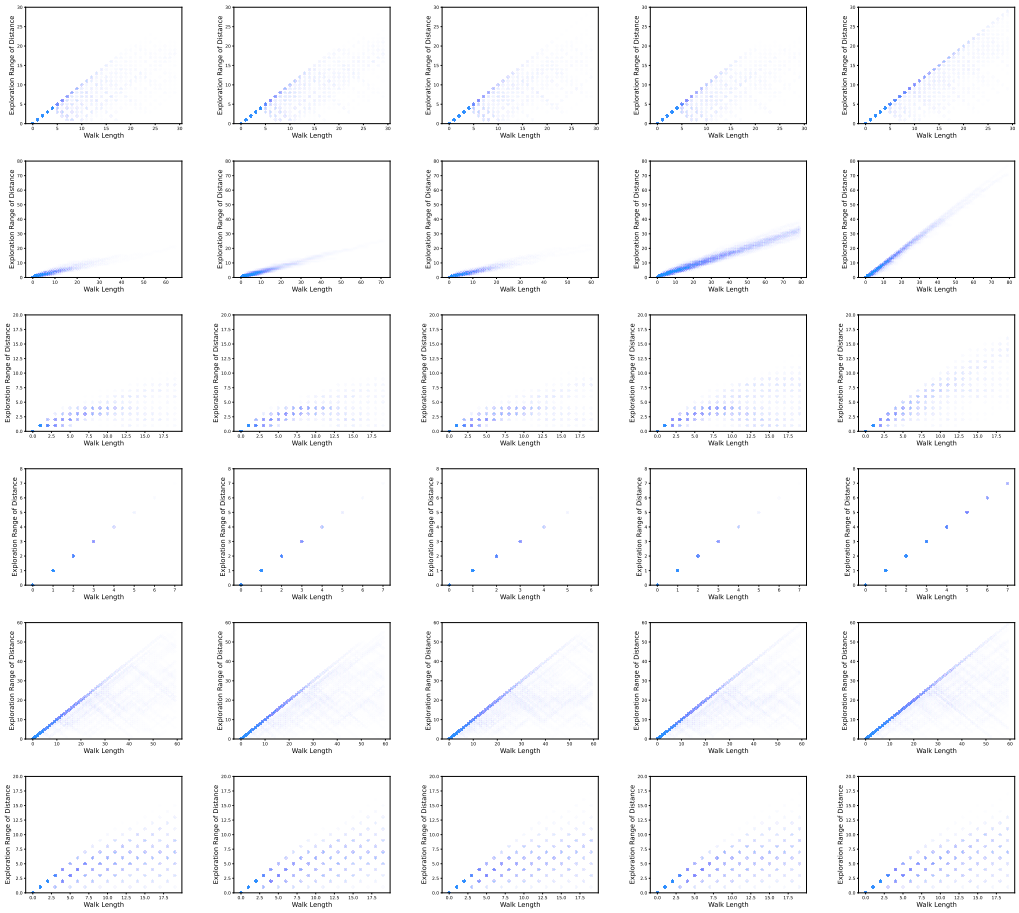

Figure 7: Exploration range of distance when taking different walk strategies tested on six synthetic graphs. **Row from top to bottom:** different synthetic graphs including CG, TG, TCG, TRG, SG, and NG, respectively. **Column from left to right:** different walk strategies including NRW, SORW, RS, DFS-RW, BC-RW (ours.), respectively.

however, there are many final nodes (i.e., leaves) possessing trivial significance on BC walks which are insufficiently observed for calibrating their distance relations well.

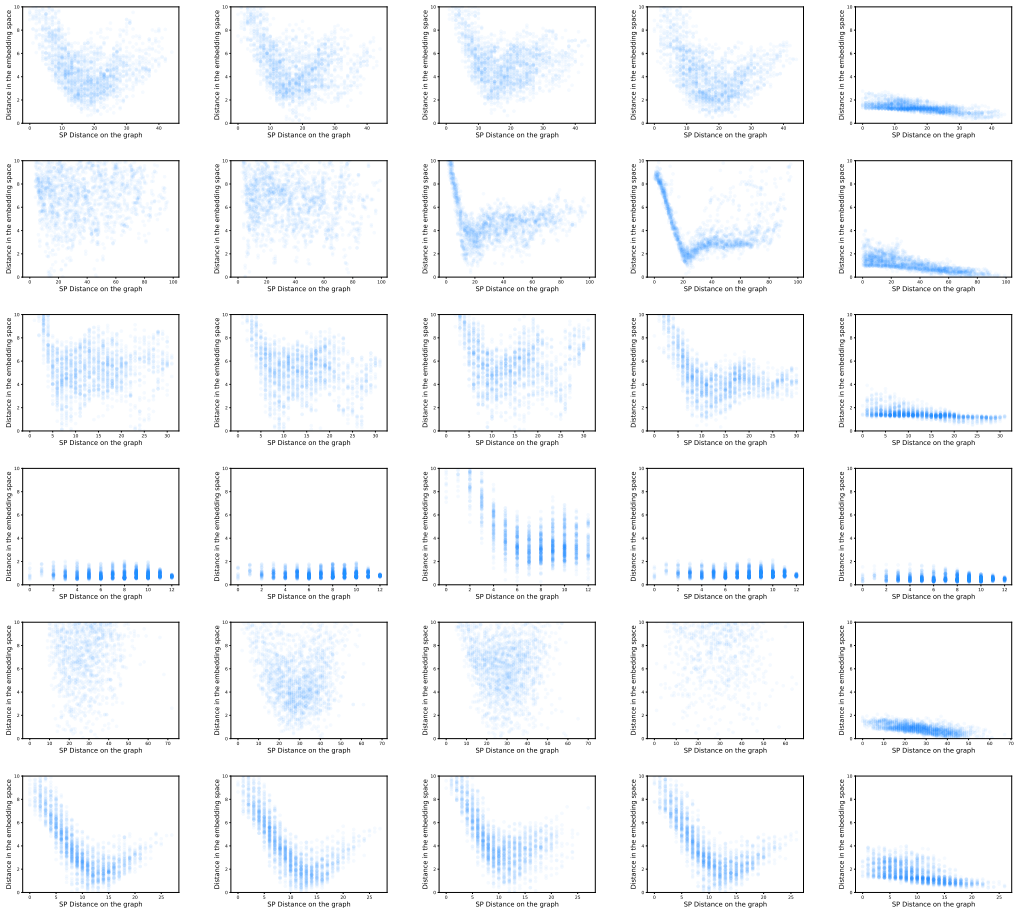

Figure 8: Measured distance from the embedding space and the original graph. **Row from top to bottom:** different graphs including CG, TG, TCG, TRG, SG, and NG, respectively. **Column from left to right:** embeddings learned by different walk strategies,i.e., NRW, SORW, RS, DFS-RW, and BC-RW (ours.), respectively. For ours, walk paths are further simulated by *distance resampling*.

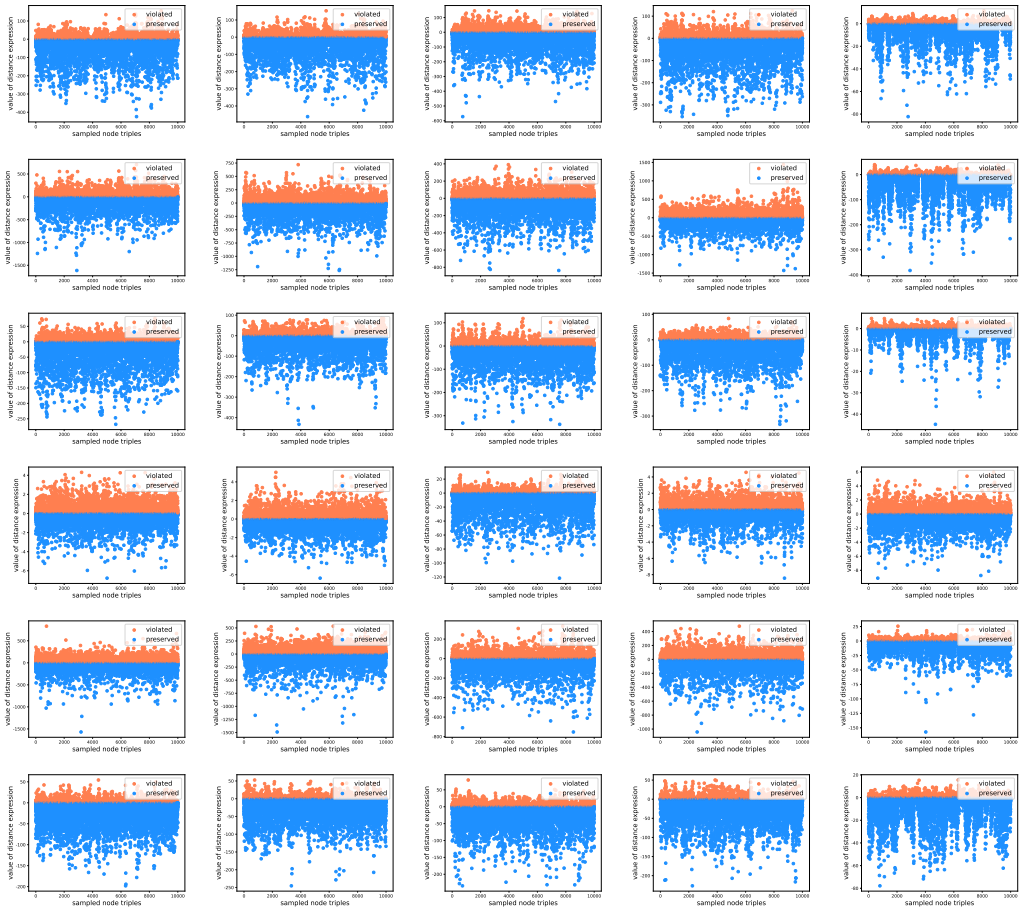

Figure 9: Distance preservation among node triplets in the embedding spaces. **Row from top to bottom:** different graphs including CG, TG, TCG, TRG, SG, and NG, respectively. **Column from left to right:** embeddings learned by different walk strategies,i.e., NRW, SORW, RS, DFS-RW, and BC-RW (ours.), respectively. For ours, walk paths are further simulated by *distance resampling*.